Review Article

Nano Research
2020, 13(7): 1842–1855

ISSN 1998-0124 CN 11-5974/O4
https://doi.org/10.1007/s12274-020-2755-3

Modulating the local coordination environment of single-atom catalysts for enhanced catalytic performance

Xinyuan Li[1,2], Hongpan Rong[1] (✉), Jiatao Zhang[1], Dingsheng Wang[2] (✉), and Yadong Li[2]

[1] *Beijing Key Laboratory of Construction-Tailorable Advanced Functional Materials and Green Applications Experimental Center of Advanced Materials, School of Materials Science & Engineering, Beijing Institute of Technology, Beijing 100081, China*
[2] *Department of Chemistry, Tsinghua University, Beijing 100084, China*

Received: 18 January 2020 / **Revised:** 10 March 2020 / **Accepted:** 11 March 2020

ABSTRACT

The local coordination environment of catalysts has been investigated for an extended period to obtain enhanced catalytic performance. Especially with the advancement of single-atom catalysts (SACs), research on the coordination environment has been advanced to the atomic level. The surrounding coordination atoms of central metal atoms play important roles in their catalytic activity, selectivity and stability. In recent years, remarkable improvements of the catalytic performance of SACs have been achieved by the tailoring of coordination atoms, coordination numbers and second- or higher-coordination shells, which provided new opportunities for the further development of SACs. In this review, the characterization of coordination environment, tailoring of the local coordination environment, and their related adjustable catalytic performance will be discussed. We hope this review will provide new insights on further research of SACs.

KEYWORDS

single-atom catalysts, coordination environment, catalytic performance, energy conversion

1 Introduction

The problem of energy shortage is especially crucial for human beings in recent years. Efficient exploration and utilization of the earth's existed fossil sources are some of the most reasonable strategies to release the energy problem. Human beings' ability to convert the existed fossil sources to clean energy will influence the industrial development and humans' daily life, which are significantly depended on the catalytic activity of catalysts [1–3]. Hence, in past decades, researchers have paid great effort on the development of new catalysts including heterogeneous and homogeneous catalysts. As for homogeneous catalysts, manipulating active metal centers and their surrounding coordination atoms are effective strategies to improve the catalytic activity and selectivity [4], which are equally important to the catalytic properties of traditional heterogeneous catalysts due to the mixed coordination environments between catalytic metal particles and supports [5–7]. However, the inevitable size dispersion of metal nanoparticles could also weaken the catalytic selectivity as well as the atomic utilization [1, 8]. The development of new catalysts with improved catalytic properties is one of the most important subjects in chemistry and catalysis.

Single-atom catalysts (SACs) could combine the advantages of both homogeneous and heterogeneous catalysts, which were designed and put forward in last century and were newly specified and developed by many groups in the last decade [1, 2, 6–14]. The SACs featured atomic dispersed metal atoms loaded on supports can exhibit comparable atom utilizations and the property of controllable coordination environment with homogeneous catalysts [15–18]. Besides, the uniform atomic active sites achieved by flexible synthesis strategies exhibit high selectivity in many important reactions such as propane dehydrogenation [19, 20], C–H bond oxidation [11, 21], O_2 reduction [22, 23], N_2 fixation [24, 25] and CO_2 reduction [26–29] etc. To date, the study on SACs has been advanced to consider the coordination environment of central metal atoms at atomic level with help from the high-resolution characterization technologies [7, 10, 30]. In most circumstance, the central metal atoms of SACs were fixed on supports by coordination bonds with N, S, O, etc. atoms from support materials or metal–metal bonds (Scheme 1). The electronic and geometric structures of central metal atoms could be adjustable by tailoring

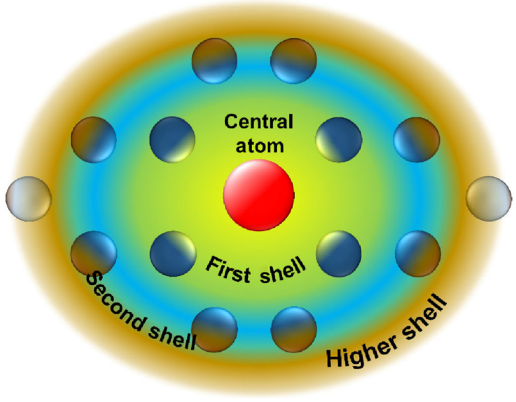

Scheme 1 Schematic illustration of central metal atom and its coordination environment.

Address correspondence to Hongpan Rong, rhp@bit.edu.cn; Dingsheng Wang, wangdingsheng@mail.tsinghua.edu.cn

the coordination environment, which would change the absorption activity of reactants on metal atoms and thus influence the catalytic properties [5, 31–34]. A comprehensive review on modulating the local coordination of SACs and their related enhanced catalytic performance is timely important.

In this review, we will first introduce the characterization technologies of coordination environment, which is vital for further investigations of SACs. Then, the local coordination environment of SACs and their influence of catalytic performance will be illustrated from some representative publications, which are categorized by macroscopic support materials (Section 3.1), specific coordination atoms (Section 3.2), and complicated second- and higher-coordination shell (Section 3.3). Finally, the future challenges and opportunities for modulating the coordination environment of SACs are forecasted.

2 Characterization of coordination environment

In the early days, the characterizations of the coordination environment were rare, owing to the lack of advanced characterization technologies. However, due to the development from traditional bulk catalysts to atomic engineered new catalysts, the analysis of the coordination environment of central metal atoms and its significant influence on the investigation of catalytic performance has been emphasized. One vital technology to analyze the coordination environment of the metallic complex is nuclear magnetic resonance (NMR). The chemical shift exhibited on NMR spectra indicated the different coordination environments. For example, Zhang et al. applied ^{31}P NMR and ^{1}H NMR to characterize the coordination abilities between metal cations and phosphines (or thiols/benzenes) (as illustrated in Fig. 1(a)) [35–37]. The chemical shift of the NMR spectrum could reflect the coordination abilities between metal cations and ligands. As for solid-state catalysts with supported metal atoms or nanoparticles, the X-ray derived spectroscopies (include X-ray photoelectron spectroscopy (XPS), X-ray absorption near edge spectroscopy (XANES) and extended X-ray absorption fine structure (EXAFS) spectroscopy techniques) are most essential approaches to characterize their coordination environments. Metal atoms coordinated by different atoms from the support will exhibit different binding energies characterized by XPS and XANES. The coordination atoms and valence states of central metal atoms could be concluded by the fitting of the spectra and concerning the XPS database [38]. In Wang's study, the difference of Fe–S, Co–S and Ni–S coordination could be determined based on the different binding energies of S 2p detected by high-resolution XPS (as illustrated in Fig. 1(b)) [39]. For further detailed characterization, EXAFS is the key technology to analyze the coordination environment, especially for single atomic catalysts. The different coordination environments of central metal atoms would exhibit different bond distances (R shift exhibited in Fourier transform (FT) functions of the EXAFS spectra). Also, the absence of the signal of the metal–metal bond is critical evidence to define a SACs. For example, Wang et al. reported the coordination environment of W atoms supported on metal-organic framework (MOF)-derived N-doped carbon (Fig. 1(c)) [40]. By comparing the k^3-weight FT-EXAFS curves of the W SAC with samples made of W–W, W–O, W–N, and W–C bonds, single atomically dispersed W catalysts could be determined.

To further evaluate the coordination environments of active sites, *in situ* characterizations could provide more valuable information during dynamic changes [41, 42]. Basically, *in situ* X-ray absorption spectroscopy (XAS) could be utilized to indicate the evolution of the coordination environment during the synthesis process. For example, Corma et al. determined the reversible transformation from Pt single atoms to nanoparticles supported on high-silica chabazite zeolite by the combination of *in situ* XAFS and XANES [43].

Besides the essential characterization during the synthesis process, *in situ* characterizations also played an important role in determining the coordination environments of active sites during the catalytic process. For example, Yang et al. investigated the coordination environment of two kinds of Pt_3Ni nanoframe during oxygen reduction reaction (ORR) by *in situ* XANES and XAFS [44]. The different coordination environments of two Pt_3Ni catalysts characterized by *in situ* XAFS at working potentials illustrated their differed performance and stabilities in the ORR process. Similarly, Xing et al. applied *in situ* XANES to evaluate the coordination environment of Fe SA/CN under various potentials, which illustrated the real active sites and reaction pathways in the ORR process [45]. Besides ORR, *in situ* XAS at working atmospheres and temperatures was

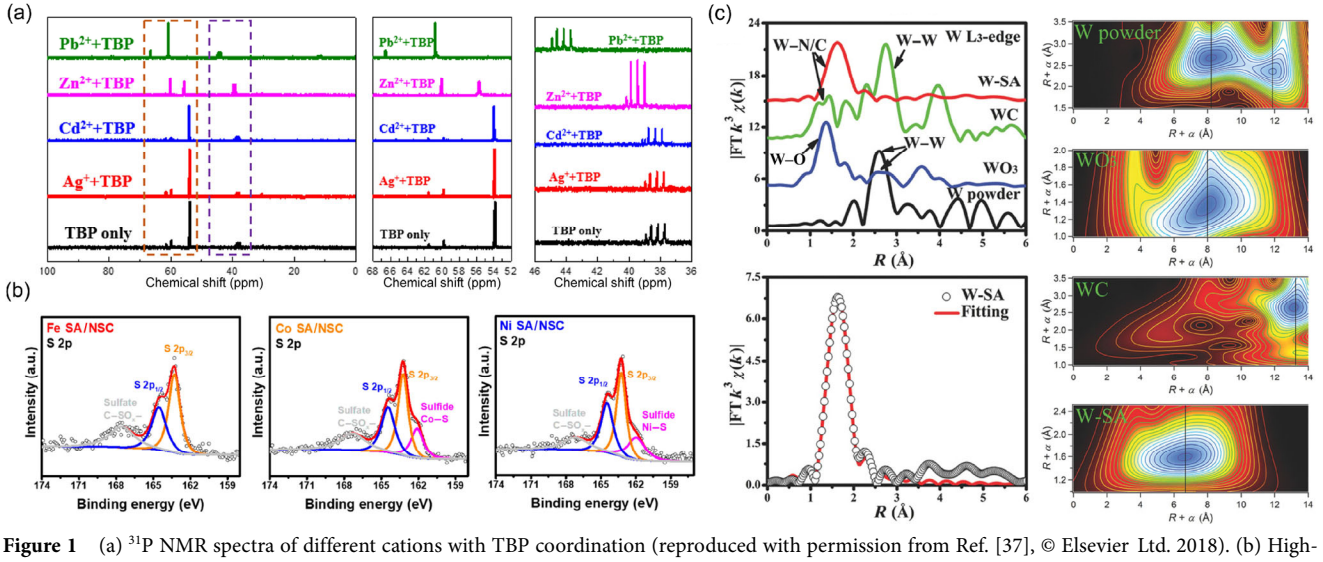

Figure 1 (a) ^{31}P NMR spectra of different cations with TBP coordination (reproduced with permission from Ref. [37], © Elsevier Ltd. 2018). (b) High-resolution XPS spectra of S 2p in Fe SA/NSC, Co SA/NSC, and Ni SA/NSC, respectively (reproduced with permission from Ref. [39], © American Chemical Society 2019). (c) k^3-weight FT-EXAFS curves of the W SAC at W L_3-edge, WT-EXAFS of the W SAC and the references and k^3-weight FT-EXAFS fitting curves of the W SAC at W L_3-edge (reproduced with permission from Ref. [40], © Wiley-VCH Verlag GmbH & Co. KGaA, Weinheim 2018).

also applied to studies of the coordination environments of another heterogeneous catalysis. For example, Zeng et al. revealed the adsorption properties of H_2 and CO on the surface of Rh SA/CoO during hydroformylation reaction by *in situ* XPS and diffuse reflectance infrared Fourier transform [46].

Besides the *in situ* XAS, *in situ* transmission electron microscopy (TEM) was also applied to analyze the coordination environment of SACs. For example, *in situ* environmental TEM and scanning transmission electron microscopy (STEM) were utilized to characterize the transformation from nanoparticles to single atoms [47, 48]. Suenaga et al. reported the characterization of coordination environment and migration of Re/Au atoms on single-layer MoS_2 support by *in situ* annular dark-field STEM [49], which provided with new opportunities for direct observations of the interactions between single atoms and coordination environments. Christopher et al. reported that the dynamic response of Pt single atoms anchored on TiO_2 was characterized by *in situ* aberration-corrected STEM [50]. The mobility of Pt atoms when heated at a high temperature within H_2 atmosphere characterized by *in situ* aberration-corrected STEM enlightened us to understand the coordination behavior of SACs further. Hence, further applications of *in situ* techniques could provide with more insightful investigations of catalytic mechanisms.

To further investigate the coordination environment of SACs, theoretical predictions are significant to optimize the coordination environments for high catalytic performance. For example, Zeng et al. reported the evaluations of activities of graphene-based SACs with different nitrogen coordination numbers for ORR, oxygen evolution reaction (OER), and hydrogen evolution reaction (HER) in theoretical insights [51]. They reported that the optimal coordination environment could be Fe-pyridine/pyrrole-N_4 for ORR, Co-pyrrole-N_4 for OER, and Mn-pyrrole-N_4 for HER, which could help design synthesis of SACs with organized coordination environments. In a recent publication by Wang et al., the N coordination effects of Mn-N_x SACs for ORR were also explored based on density functional theory (DFT) calculations [52]. They reported that Mn-N_4/C could be an attractive candidate, which positioned near the apex of the volcano plot with a η_{SHE} of 0.33 V.

Li et al. reported a comprehensive theoretical study of M SA/FeO_x (M = Pd, Pt, Ni, Fe, Co, Cu; Ru, Rh, Ag, Os, Ir, Au, etc.), and they found a close relationship between the catalytic activity of M SA/FeO_x for CO oxidation and their coordination environments [34]. In their study, Pd SA/FeO_x could be the best candidates for further applications, which even exhibited better performance than reported Pt SA/FeO_x and Ni SA/FeO_x. Based on the theoretical studies, further precise characterizations such as coordination number, the second- and higher-shell coordinations were mostly performed by combining experimental XAS spectra and theoretical modelings [31, 53]. For example, Jaouen et al. reported that the identification of Fe-SA/N_4C_{12}, Fe-SA/N_4C_{10}, and Fe-SA/$N_4C_{12}O_x$ could be indicated by experimental XANES and related theoretical spectra [54]. Similarly, W-N_1C_3 (Fig. 1(c)) and Fe-Cl_1N_4 coordination could also be distinguished separately by comparing the EXAFS spectra and corresponding fitting curves in *R* spaces as reported by Wang et al. [40, 55]. This strategy could also be applied to predict the higher-shell coordination of Cu-N_4-C_8S_2, as reported by Zhang et al. [38]. Further investigation on higher-shell coordination requires more precise characterization and a deeper theoretical basis.

3 Local coordination environment of SACs

In most reported SACs, metal atoms usually are chemically anchored on the support materials, which could directly influence the stability and catalytic performance of center metal atoms. In this section, we will firstly discuss the alternation of coordination components, with emphasis on the classifications of substrates. Then, we will discuss the adjustment of coordination number according to the types of coordination atoms along with dual atom coordination. Finally, we will briefly discuss the present studies on SACs with second- and higher-coordination shell and their enhanced catalytic performance.

3.1 Coordination components

The different coordinating abilities between central metal atoms and support atoms could be utilized in mediating the catalytic activity of metal atoms. Based on this, the support materials of SACs played essential roles in their catalytic performance. The direct coordination between support atoms and central metal atoms could be categorized as first-shell coordination. In this section, by view of the support materials, some common coordination components in first-shell coordination will be introduced, such as carbon materials (mainly N doped carbon materials with first-shell N coordinated), metal oxides (with first-shell O coordinated), metal sulfides (with first-shell S coordinated) and metallic materials (including alloys and intermetallic materials, with first-shell metal atoms coordinated).

3.1.1 *SACs supported on carbon materials*

Carbon materials are important supports for various catalytic reactions due to their properties of low cost, high conductivity, and easy modification. As for pure carbon materials as substrates of SACs, most active atoms are selectively embedded on the defects of carbon substrates, which exhibited as carbon coordinated SACs. For example, single metal atoms such as Ni, Pd and Pt metal atoms embedded on pure graphene or graphdiyne have been reported by Chen et al. [56], Lu et al. [57] and Lu et al. [58]. However, due to the low binding energy between C and metal atoms (the lack of lone electron pair in C atom), SACs on pure carbon substrates usually are synthesized at high annealing temperature and feature low loading amount. To further mediate the coordination environment of SACs supported on carbon materials, doping other atoms with higher binding energy is an efficient strategy. For example, N-doped carbon materials, including N-doped graphene, C_3N_4, and metal-organic framework derived N-doped carbon materials, are applied as important N first-shell coordinated support for SACs with high metal loading amount. Compared to C atom, N atom features one more electron in the valence electron shell, which provides higher binding energy. For example, Li et al. reported a cocoon silk chemistry strategy to synthesize ultrathin N-doped carbon nanosheets with high nitrogen content (20.47 wt.%) and high specific surface area (2,105 $m^2 \cdot g^{-1}$), which are ideal substrates for anchoring metal atoms (Fig. 2(a)). The as-prepared Co SA/CN catalysts exhibited high activity on the C–H bond activation [59]. Similarly, Song et al. reported a Co SA/CN by applying g-C_3N_4 as a substrate, which exhibited superior activity for transfer hydrogenation of nitrobenzene [60]. As for two-dimensional (2D) N-doped carbon substrates, N-doped graphene is an attractive support for high metal loading and appropriate coordination ability. Zhang et al. reported the synthesis of Pd SA/N-doped graphene, which exhibited highly selective photothermal hydrogenation of acetylene to ethylene [61]. Wang et al. reported Ni SA/N-doped graphene for highly efficient electrocatalytic CO_2 reduction with 95% selection of CO [62]. Both of the two mentioned SACs on N-doped graphene could be simply achieved by wet impregnation strategy. Xiang et al. also reported a pyrolysis free pathway to

synthesize Fe SA/N-doped graphene, which exhibited high ORR efficiency [63].

Based on the higher binding energy between N and metal atoms and spatial confinement effects, MOFs with N-containing coordinated links are also attractive substrates for SACs [6]. A straightforward strategy to synthesize MOFs-derived SACs on N-doped carbon substrates is by pyrolysis of metal ions based or encapsulated MOFs. SACs such as Co, W, and Bi SA/CN derived from predesigned MOFs have been investigated by Wang et al. [40], Wu et al. [64], Spendelow et al. [65] and Zhang et al. [47]. Besides, MOFs could also be applied as host to capture active metal precursors. For example, Wang et al. reported the synthesis of atomic dispersed Ru clusters within MOFs (Fig. 2(b)). The applied ZIF-8 shell could achieve regioselective catalysis, which exhibited high selectivity in hydrogenation of acetylene to ethane [66]. To further versatile synthesis of such SACs, Li et al. reported the ionic exchange of MOFs to achieve Ni SACs, which exhibited efficient electroreduction of CO_2 (Fig. 2(c)) [67]. Taking advantages of the coordination between N and metal atoms, Wang et al. reported synthesis of Co SACs anchored on hollow N-doped carbon spheres by template-assisted pyrolysis method (Fig. 2(d)) [68]. The firstly prepared SiO_2 spheres were dispersed in metalloporphyrins solutions, followed by pyrolysis. Similar strategies have been applied to the synthesis of Fe, Co, Ni, Mn SA/CN (Fig. 2(e)) [26, 69, 70]. However, it has to be mentioned that the examples presented above only focusing on SACs with mostly coordination number of 4. Since the further alternation of N coordination numbers and dual coordination atoms (by modified central atoms with S, Cl and P etc.) are also important factors for catalytic performance, we will systematically discuss them in Sections 3.2.1 and 3.2.2.

3.1.2 *SACs supported on metal oxides*

Compared to carbon substrates, metal oxide substrates such as FeO_x, TiO_2, SiO_2, CeO_2 are also widely applied in industrial catalytic fields. Their surface defects could be applied to anchor metal atoms to synthesize SACs. Liu et al. reported the Pt SA anchored on defects of FeO_x substrate by wet co-precipitation [9]. The as-prepared Pt SA/FeO_x catalysts exhibited high activity for both CO oxidation and preferential oxidation of CO in H_2 due to the appropriate coordination environment. In their following research, they reported the Ir SA/FeO_x for remarkable catalysis on water gas shift reaction [71]. Zheng et al. reported a photochemical route to synthesize Pd SA/TiO_2 SACs by applying ultrathin TiO_2 nanosheets with a high density of defects as substrate [72]. The ethylene glycolate and UV light irradiation supplied with a mediate reduction environment, which facilitated a high single atom loading (1.4 wt.%). Based on the surface defects engineering, Wang et al. firstly constructed oxygen vacancies on the TiO_2 surface, and then prepared stable and high loading Au SA/TiO_2 SACs by co-precipitation (Fig. 3(a)), which exhibited a majority of Au–O coordination [73]. Li et al. reported the synthesis of Pt SA/TiO_2 SACs by electrostatic-induction ion exchange and two-dimensional confinement strategy (Fig. 3(b)) [74, 75]. The as-prepared Pt SA/TiO_2 exhibited enhanced anti-Markovnikov alkene hydrosilylation and photocatalytic hydrogen generation properties. Similarly, many metal oxide-based SACs were synthesized by the co-precipitation or electrostatic adsorption, such as Rh SA/TiO_2 [76], Pt SA/Fe_2O_3

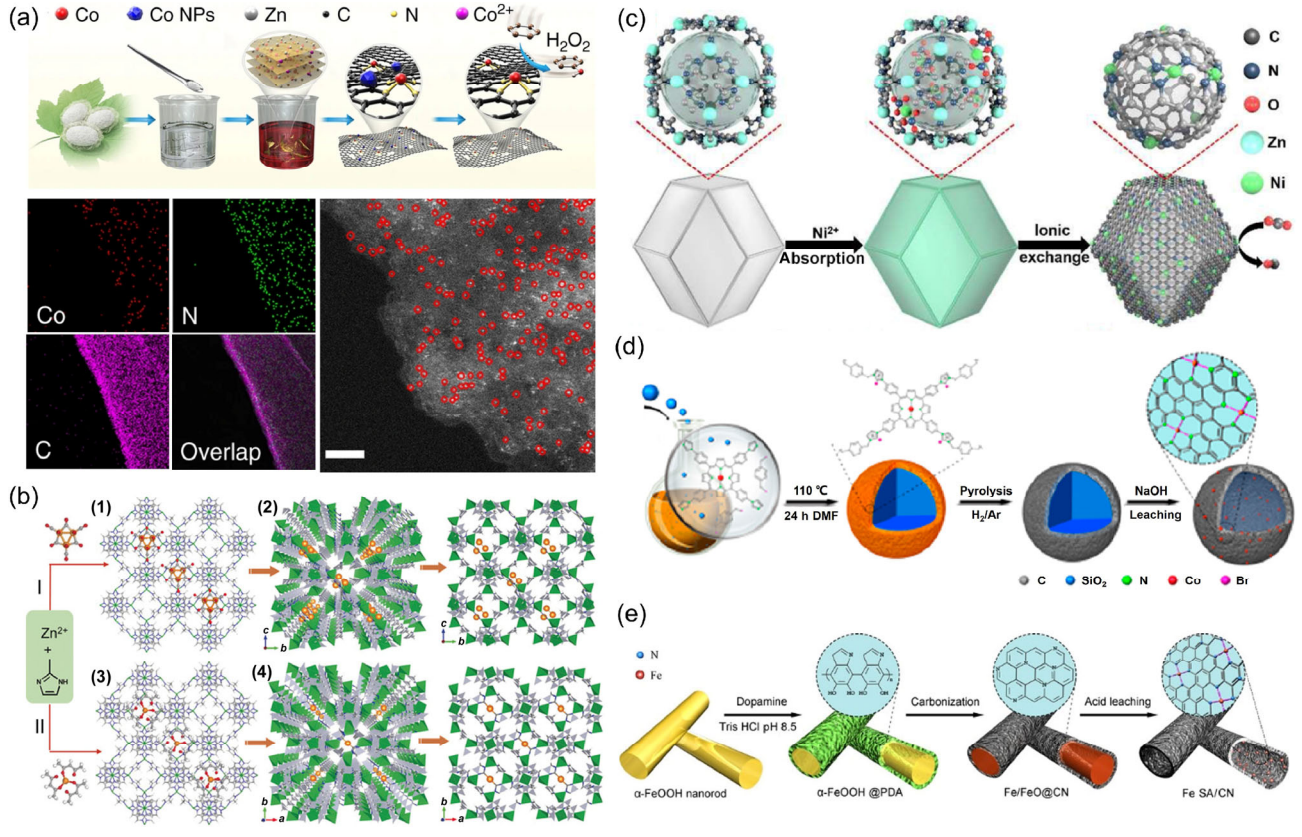

Figure 2 (a) Synthesis strategies of Co SA/CN catalyst, corresponding energy-dispersive X-ray spectroscopy (EDS) elemental mapping and aberration corrected high-angle annular dark-field (HAADF)-STEM image (reproduced with permission from Ref. [59], © Zhu, Y. Q. et al. 2018). (b) Schematic preparation process of Ru_3@ZIF-8 and Ru_1@ZIF-8 catalyst (reproduced with permission from Ref. [66], © Wiley-VCH Verlag GmbH & Co. KGaA, Weinheim 2019). (c) Schematic illustration of the synthesis of Ni SA/NC (reproduced with permission from Ref. [67], © American Chemical Society 2017). (d) Schematic illustration of the synthesis of Co SA/hollow N doped carbon sphere (reproduced with permission from Ref. [68], © American Chemical Society 2017). (e) Schematic illustration of the synthesis of Fe SA/CN (reproduced with permission from Ref. [69], © American Chemical Society 2017).

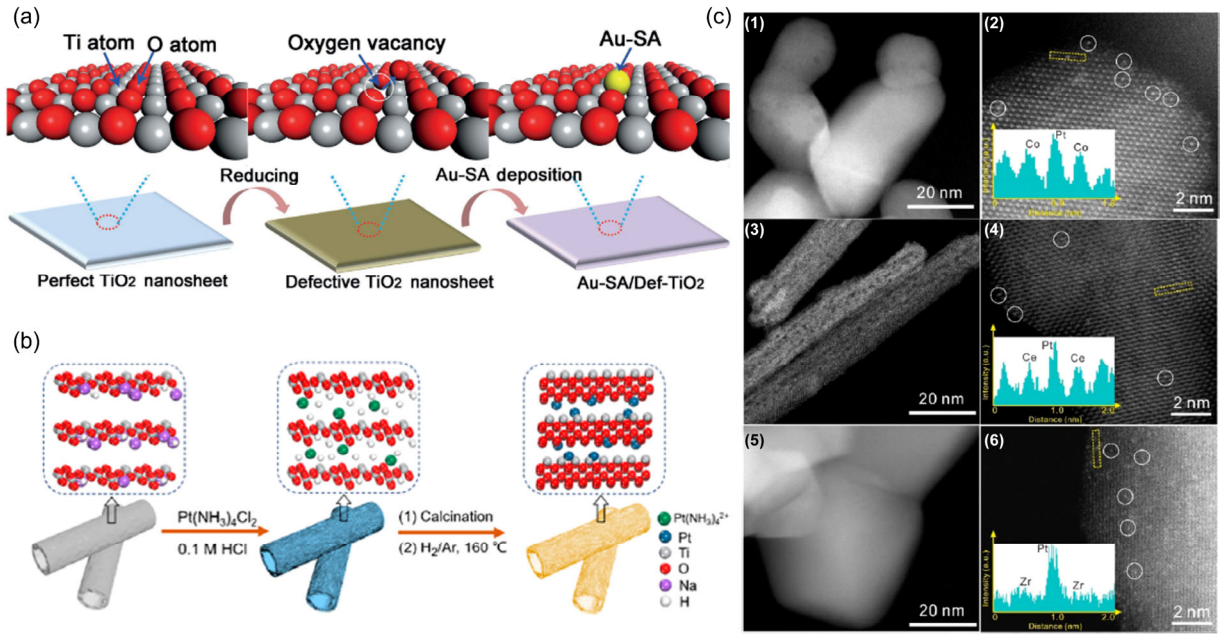

Figure 3 (a) Schematic illustration of the synthesis of Au SA/TiO_2 (reproduced with permission from Ref. [73], © Wiley-VCH Verlag GmbH & Co. KGaA, Weinheim 2018). (b) Schematic illustration of the synthesis of $Pt_1^{\delta+}$ SA/TiO_2 (reproduced with permission from Ref. [70], © Wiley-VCH Verlag GmbH & Co. KGaA, Weinheim 2019). (c) Aberration-corrected HAADF-STEM images of Pt_1/Co_3O_4, Pt_1/CeO_2, and Pt_1/ZrO_2 (reproduced with permission from Ref. [84], © American Chemical Society 2019).

[77], Pt SA/WO_{3-x} [78], Pt SA/CeO_2 [79, 80], Pd SA/CeO_2 [81], Pd SA/Cu_2O [82], Au SA/CuO [83], Pt SA/ZrO_2 [84] and Pt SA/$Ni(OH)_x$ [85] (Fig. 3(c)) reported by many research groups in SACs. The charge transfer from metal oxide support to central metal atoms could facilitate the enhanced catalytic performance, which has widely utilized for industrial applications.

3.1.3 *SACs supported on metal sulfides*

Different from the aforementioned N-doped carbon and metal oxide substrates, metal sulfides provided with appropriate band gap and higher binding energy with metal atoms, which are important candidates for photocatalytic and electrocatalytic applications [86, 87]. Single metal atoms could be loaded on metal sulfides substrates (especially transition metal dichalcogenides), which could exhibit outstanding performance due to the catalytic activity, trapping of charge carriers and comprehensive surface modifications [87–89]. For example, Suenaga et al. reported the characterization of a single atomic site doping of Re and Au on MoS_2 nanosheets [49]. By analyzing the interaction between doping atoms and host, the authors proved that the single atomic doping could enhance the chemical affinity of the system, which could be utilized for further applications on nano-electronic devices. Warner et al. reported that Pt atoms could localize on S vacancies and exhibit dynamic hopping to nearby vacancy sites [90]. They further indicated that Pt atoms could influence the hydrogen evolution reactions by varying the hydrogen adsorption energy. In a related publication by Bao et al., Pt SA/MoS_2 exhibited enhanced hydrogen evolution reaction catalytic abilities, which could be owing to the tuned adsorption of H atoms by Pt atoms [12]. Besides, Tsang et al. reported the synthesis of Co SA/MoS_2, which exhibited superior activity, selectivity, and stability for the hydrodeoxygenation of 4-methylphenol to toluene compared with conventional $CoMoS_2$ catalysts [91]. The enhanced activity could be achieved by the observed Co–S–Mo interfacial sites.

Besides the deposition of single atoms on the surficial defects of metal sulfide substrates, single atomic site doping could also be applied to achieve functional modification. As reported by Zhang et al., single atomic site Ag^+ or Cu^+ doped CdX and ZnX (X = S, Se, Te) quantum dots were synthesized via phosphine facilitated cation exchange reactions from Ag_2X QDs (Fig. 4(a)) [35, 36]. The atomic site doping was further examined by high-resolution TEM (HRTEM) and EXAFS [92]. The similar cation exchange reactions can also be applied to synthesize metal-semiconductor core–shell nanocrystals with stable atomic doped shell and atomic organized hetero-interface [37, 93]. In their recent publication, the semiconductor shell with the atomic dopant could be tailored from n- to p-type by cation exchange reactions [94]. The as-prepared Au@CdS core–shell nanocrystals with Cu SA dopants exhibited promising photoelectrochemical hydrogen evolution property. Similarly, cation exchange reactions could be applied to achieve metal-sulfide nanocrystals (NCs) with high single atomic loadings. Li et al. reported the synthesis of single atomic Pt sites on

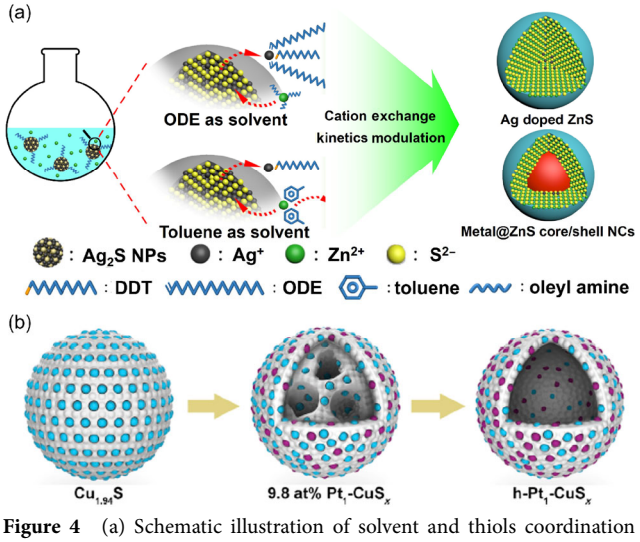

Figure 4 (a) Schematic illustration of solvent and thiols coordination facilitated cation exchange reactions enabled the synthesis of Ag single atomic doped ZnS nanocrystals (reproduced with permission from Ref. [36], © Wiley-VCH Verlag GmbH & Co. KGaA, Weinheim 2019). (b) Schematic illustration of the structure evolution of Pt_1 SA/CuS_x (reproduced with permission from Ref. [95], © Elsevier Inc. 2019).

hollow Cu_xS nanocrystals, which exhibited highly selective O_2 reduction to H_2O_2 in acid solution (Fig. 4(b)) [95].

3.1.4 *SACs supported on metal substrates*

The catalytic properties of noble metal materials could significantly differ from their size and morphologies as the size reduces to nanoscale or atomic level. Located noble single metal atoms on noble metal substrates could exhibit enhanced catalytic performance due to the synergistic effect of isolated noble metal atoms and their coupling with metal substrates [96]. Most reported single atoms are anchored on alloys, or intermetallic nanocrystals, namely single atom alloys (SAAs), which are mostly achieved by the different surface potentials of metal atoms facilitated adsorption. Toshima et al. reported Au isolated atoms on Pd nanoclusters SAA, which exhibited enhanced catalytic activity on aerobic glucose oxidation [97]. Zhang et al. reported Pd SA on Ag nanoparticles SAA anchored on SiO_2 substrates for highly selective hydrogenation of acetylene to ethylene in excess ethylene [98]. As for morphology tailoring, Hong et al. reported the atomically dispersed Ru on ultrathin Pd nanoribbons, which exhibited enhanced property of hydrogenolysis in chemoselective hydrogenation of C=C bonds [96]. The Cu pair atoms on $Pd_{10}Te_3$ alloyed nanowires also exhibited efficient and selective electrochemical reduction of CO_2, as reported by Chen et al. (Figs. 5(a) and 5(b)) [28]. Similarly, Wang et al. reported the anchoring of isolated Co single atoms into the lattice of Ru nanoplatelets, which exhibited accelerated water dissociation kinetics [99].

Besides, some highly active atoms for H_2 activation (such as Pt) suffering from inactivation by C accumulation, could be anchored on substrates with reduced binding strength for C species (such as Cu). In a publication reported by Sykes et al., Pt SA/Cu SAAs with an atomic ratio of Pt:Cu = 1:1.25 exhibited excellent CO tolerance in H_2 activation [100]. In their further publication, they prepared Pt/Cu single atom alloys which exhibited efficient and highly selective C–H activation catalytic property [20]. Compared to Pt nanoparticles, the Pt/Cu single atom alloys exhibited intermediate barriers for C–H activation, which kept active but prevented from coking. Nearly at the same time, Gong et al. reported Pt/Cu single atom alloys could promote the desorption of surface-bonded propylene and prohibit its further dehydrogenation, resulting in high propylene selectivity (~ 90%) [19]. In a recent publication by Wu et al., Ru single atoms were localized on PtCu alloys [101]. The engineered electronic structure of Ru single atoms by tailoring the Cu-Pt ratio of substrates facilitated the enhancement of acidic water oxidation for electrocatalysis. Similarly, atomic dispersed Sn in Pt_3Sn intermetallic nanocrystals enhanced the activity and stability of electrochemical reactions (Fig. 5(c)) [102].

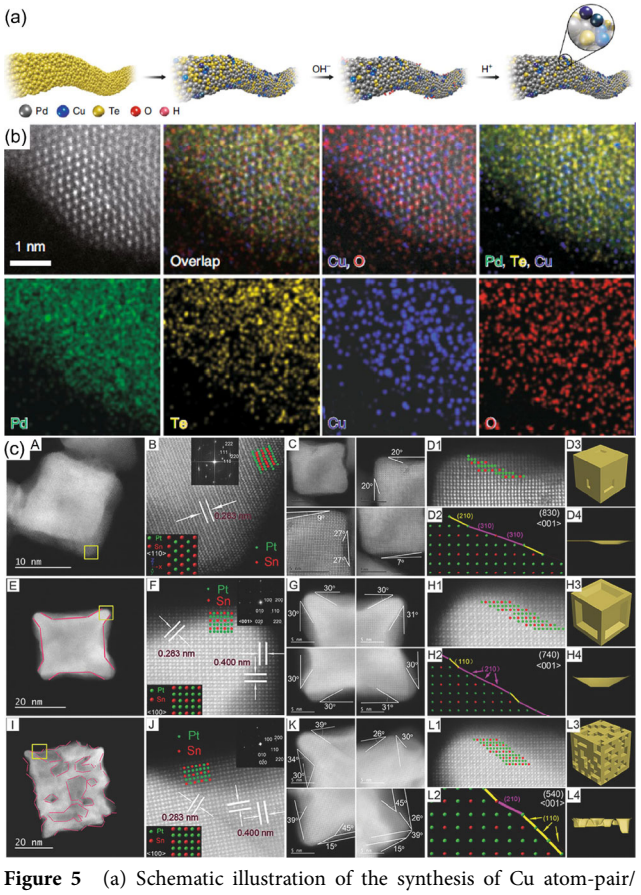

Figure 5 (a) Schematic illustration of the synthesis of Cu atom-pair/$Pd_{10}Te_3$ nanowires and (b) atomic-resolution EDS mapping images (reproduced with permission from Ref. [28], © Springer Nature 2019). (c) Atomic-resolution HAADF-STEM images and corresponding schematic illustrations of cubic (A–D), concave cubic (E–H), and defect-rich cubic intermetallic (I–L) Pt_3Sn nanocrystal (reproduced with permission from Ref. [102], © Wiley-VCH Verlag GmbH & Co. KGaA, Weinheim 2016).

3.2 Adjustment of coordination atoms

To further optimize the catalytic performance of SACs, the coordination number of active metal single atoms were also systematically investigated, which could significantly influence the catalytic properties of SACs. The coordination number mainly depends on the valence state of metal atoms and their coordination environment. The reported adjustment of coordination atoms mainly includes the N coordination, O coordination, and dual atom coordination, and we discuss them in the following sub-sections.

3.2.1 *Adjustment of N coordination*

The common coordination number of metal atoms with N atoms is 4, which could be attributed to the valence state and electronic structures of central atoms. For example, Bao et al. reported the synthesis of Fe-N_4/graphene SACs for catalytic oxidation of benzene by ball milling of Fe-phthalocyanine (FePc) with graphene nanosheets [11]. The Fe-N_4 coordination provided with a potential bonding of Fe=O, which was indicated as a key step to promote the conversion of benzene to phenol. In their further study, Bao et al. reported the synthesis of Cu^I-N sites SACs by mixing CuPc with dicyandiamide for efficient ORR in alkaline medium [103]. By adjusting the pyrolysis temperature, Zhang et al. successfully synthesized Fe-N_x (x = 4–6) SACs, among which Fe^{III}-N_5 exhibited the highest selective oxidation of C–H bond turnover frequency (TOF) [21]. Wang et al. also reported that Fe-N_5 SACs exhibited superior performance in electrochemical CO_2 reduction [104]. By similar strategies, Wu et al. reported the tailoring of Co-N_2, Co-N_3, and Co-N_4, while Co-N_2 exhibited both high selectivity and activity on electroreduction of CO_2 to CO (Figs. 6(a)–6(e)) [105]. Chen et al. further studied the preparation of Fe-N_xC_y (x + y = 4) and their catalytic sites in the benzene oxidation reaction, among which Fe-N_4 exhibited the highest performance (Figs. 6(f)–6(m)) [106].

Utilizing the strong coordination interaction between N and metal atoms, some metal nanoparticles or bulk materials could also be transformed into single atoms with specific N-coordination numbers during the pyrolysis process. In an impressive publication by Li et al., Cu-N_4/C SACs could be achieved by the pyrolysis of Cu foam and ZIF-8 in an ammonia atmosphere (Fig. 7(a)) [107]. The defects of the nitrogen-rich carbon support could trap the $Cu(NH_3)_x$ species efficiently, which could be applicable for scalable synthesis of SACs. The

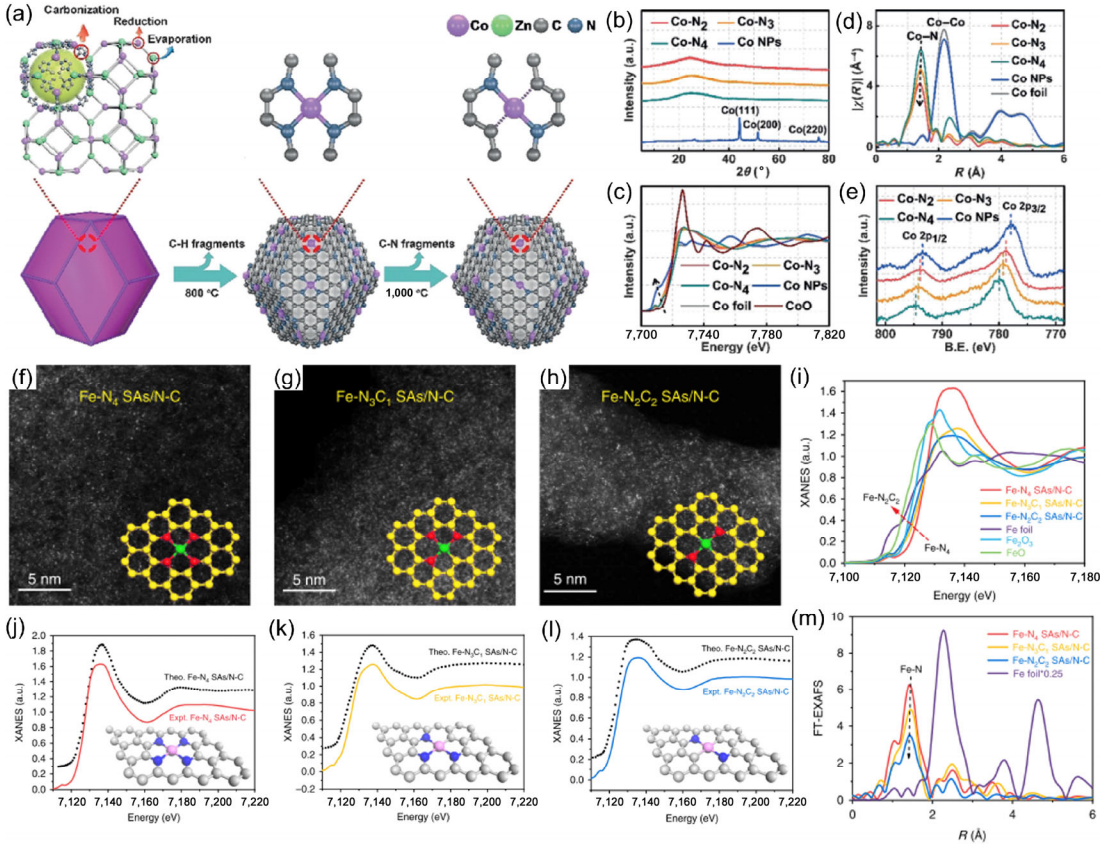

Figure 6 (a)–(e) Schematic illustration and structure characterization of the coordination tailoring of Co-N_x/CN SACs: (a) schematic illustrations of Co-N_4 and Co-N_2/CN SACs, (b) XRD pattern, (c) XANES spectra, (d) EXAFS spectra, and (e) XPS spectra of Co-N_2, Co-N_3, Co-N_4 and Co nanoparticles (reproduced with permission from Ref. [105], © Wiley-VCH Verlag GmbH & Co. KGaA, Weinheim 2018). (f)–(m) Structure characterization of Fe-N_xC_y SAs/CN: (f)–(h) AC-HAADF-STEM images, (i) XANES spectra at the Fe K-edge, (j)–(l) comparison between the experimental K-edge XANES spectra and the theoretical spectra, and (m) FT k^3-weighted $\chi(k)$-function of the EXAFS spectra of the Fe-N_4 SAs/CN, Fe-N_3C_1 SAs/CN, and Fe-N_2C_2 SAs/CN (reproduced with permission from Ref. [106], © Pan, Y. et al. 2019).

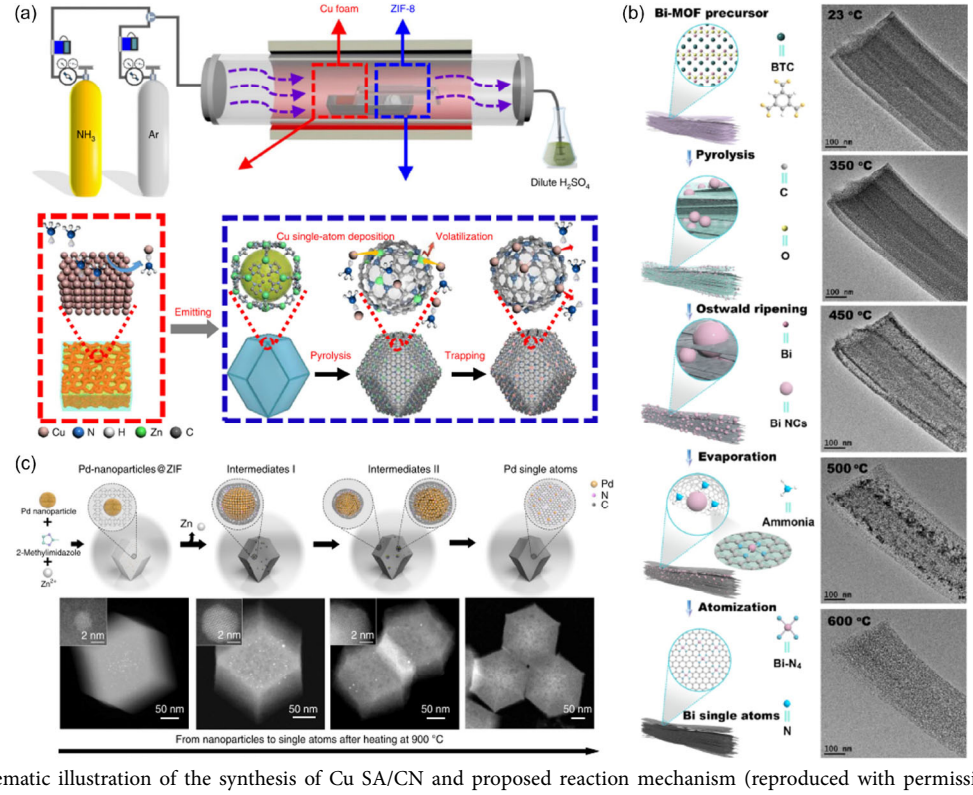

Figure 7 (a) Schematic illustration of the synthesis of Cu SA/CN and proposed reaction mechanism (reproduced with permission from Ref. [107], © Springer Nature 2018). (b) Schematic illustrations and corresponding TEM images of transformation from Bi-MOF to Bi SA/CN (reproduced with permission from Ref. [47], © American Chemical Society 2019). (c) Schematic illustrations and corresponding high-resolution HAADF-STEM images of evolution from Pd-nanoparticles@ZIF-8 to Pd SA/CN (reproduced with permission from Ref. [108], © Springer Nature 2018).

as-prepared Cu-N_4 exhibited superior ORR performance and exceptional thermal stability. In an improved strategy reported by Zhang et al., Bi-N_4/C SACs could be achieved by the pyrolysis of Bi-MOF precursor and dicyandiamide in Ar atmosphere, which featured enhanced performance for electrocatalysis for CO_2 reduction (Fig. 7(b)) [47]. Besides, single metal atoms could also be transformed from metal nanoparticles within carbon support with high nitrogen contents. For example, Li et al. reported the synthesis of Pd-, Au-, Pt-N_4/CN SACs transformed from corresponding metal nanoparticles@ZIF-8 after heating at over 900 °C (Fig. 7(c)) [108]. The as-prepared Pd-N_4/CN SACs exhibited high performance on the semi-hydrogenation of acetylene.

3.2.2 *Adjustment of oxygen coordination*

Similar to nitrogen atom, the oxygen atom is another kind of typical coordination atom, as introduced in Section 3.1.2 above. The coordination number of oxygen atoms surrounded metal atoms could also significantly influence the catalytic activity of central atoms. In a publication reported by Zhang et al., near-atomic dispersed PtO_x clusters on CeO_2 nanowires exhibited applicable low-temperature CO oxidation activity [109]. They investigated that 1.3% PtO_x/CeO_2 with low Pt–O coordination number (2.0 ± 0.3) exhibited a remarkably 1/2 order higher catalytic activity than PtO_x/CeO_2 with high Pt–O coordination number (3.1 ± 0.3). They illustrated that the increased oxygen coordination number could decrease the catalytic activity due to loss of effect active sites.

In contrast, the suitable oxygen coordination number with highly exposed Pt sites could optimize catalytic efficiency and atom utilization. Si et al. also reported that appropriate oxygen coordination numbers of Pt-O/$Ce_{0.5}Zr_{0.42}La_{0.08}O_x$ were significant for their catalytic ability of the oxidation of methane [110]. In their study, 1%Pt/$Ce_{0.5}Zr_{0.42}La_{0.08}O_x$ with appropriate Pt–O (4.8 ± 0.3) and Pt–Pt (1.6 ± 0.7) exhibited the highest catalytic performance. Corma et al. reported the tailoring of oxygen coordination number of Pt SA/high silica chabazite zeolite by adjusting sintering temperature and atmosphere, which were utilized to mediate their catalytic performance in the hydrogenation of ethylene and propylene [43]. In the recent publications, Zhang et al. and Hosono et al. separately reported that Pt SA/metal oxide with low Pt–O coordination number could achieve high hydrogenation catalytic performance [111, 112]. As for PtO_2, the coordination number of Pt–O is around 6. In the publication by Zhang et al., they reported that the increasing synthesis temperature could lead to the gradual decrease of the coordination number of Pt–O in the synthesis of Pt SA/Fe_2O_3 [111]. The as-prepared Pt SA/Fe_2O_3 (600 °C sintering) with low Pt–O coordination number (1.8) exhibited the highest TOF (3,809 $mol_{conv.}\cdot h^{-1}\cdot mol_{Pt}^{-1}$) during hydrogenation of 3-nitrostyrene, however, Pt SA/Fe_2O_3 (500 °C sintering) with higher Pt–O coordination number (3.8) exhibited relatively low TOF (491 $mol_{conv.}\cdot h^{-1}\cdot mol_{Pt}^{-1}$). They concluded that the decrease in Pt–O coordination number could decrease the oxidation state of Pt sites and meanwhile enhance their hydrogenation activity. In the publication by Hosono et al., the Pt SA/12CaO·7Al_2O_3 with a low coordination number of Pt–O (2.52) exhibited high catalytic activity (with TOF up to 25,772 h^{-1}) in chemoselective hydrogenation of nitroarenes [112].

By further studying the coordination state of SACs on oxide support, Qiao et al. reported that the single metal atoms could also be stabilized through a strong covalent metal–support interaction instead of anchoring on defect sites (Figs. 8(a) and 8(b)) [15]. They proved that the reducibility of iron oxide applied in their systems was crucial for anchoring isolated metal atoms. The findings could also be utilized to synthesize further SACs supported on metal oxides with a high amount of loadings. In a recent study, Lu et al. prepared Pt single atoms anchored on Co_3O_4 through strong electronic metal–support interactions, and they exhibited enhanced activity for dehydrogenation of ammonia borane [84]. In another publication by Li et al., due to the organized Pt–O–Ti^{3+} coordination, single Pt atoms anchored on defective TiO_2 support exhibited unprecedentedly high photocatalytic hydrogen evolution rate [75]. By modifying hydroxyl ligands of TiO_2 surface, a facile adsorption-oxidation strategy could be exploited to tune the

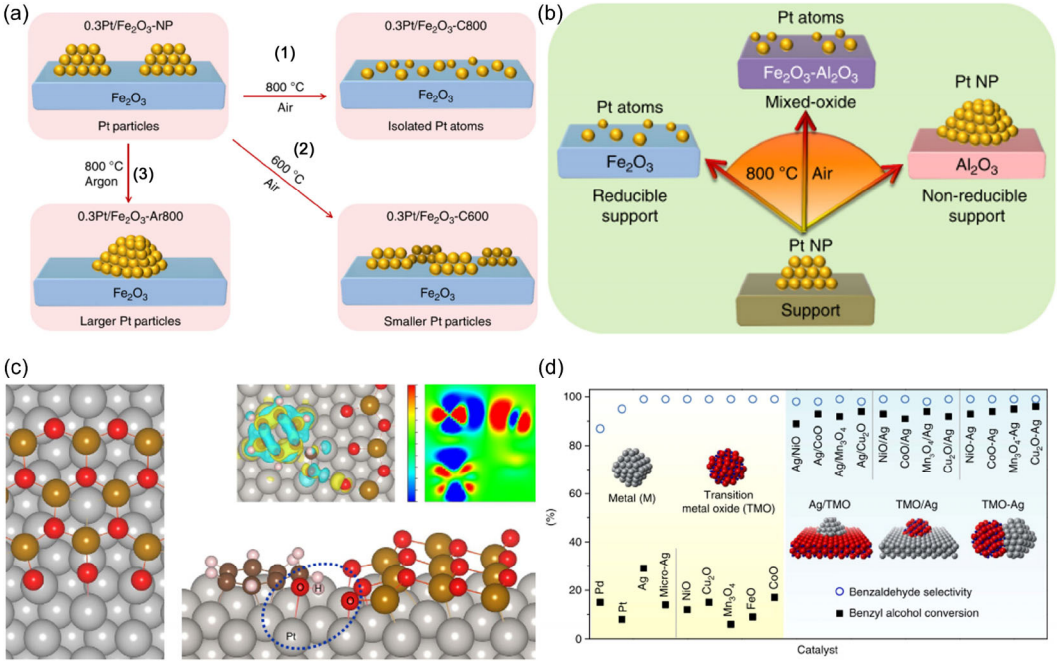

Figure 8 (a) Schematic illustration of thermally induced Pt nanoparticle restructuring and (b) their dispersion on different supports (reproduced with permission from Ref. [15]. © Lang, R. et al. 2019). (c) Schematic illustration of oxygen-terminated FeO/Pt (111) interface (O-FeO/Pt (111)) and benzyl alcohol adsorption at the O-FeO/Pt (111) interface and (d) coordination tailoring facilitated the improved catalytic performance of conversion of benzyl alcohol (solid square) and selectivity to benzaldehyde (reproduced with permission from Ref. [114], © Zhao, G. et al. 2017).

coordination number (Fe-O_3 or Fe_2-O_3) of Fe single atoms anchored on TiO_2 support [113]. The Fe central atoms with low coordination number featured low spin state, which resulted in its superior performance for OER. Besides atomic dispersed noble metal atoms anchored on metal oxide support, atomic metal oxide pair anchored on metal substrates were also investigated by Li et al., which exhibited improved catalytic property on the conversion of benzyl alcohol and their selectivity to benzaldehyde (Figs. 8(c) and 8(d)) [114]. Their study illustrated that the interfacial effect could be utilized to achieve more stable and efficient SACs.

3.2.3 *Adjustment of dual-atom coordination*

As mentioned in previous sections, multi-coordinating atoms could be applied to mediate the catalytic activity of central metal atoms. Compared to the mentioned adjustment of coordination number of nitrogen or oxygen, the adjustment of dual-atom coordination is another effective strategy to optimize their catalytic activities. For example, the aforementioned Fe-N_xC_y SACs could also be categorized as dual atom coordination, which were commonly reported in C and N supported SACs [106]. Besides the C and N coordination, other dual-atom coordination could be achieved by anchoring halogens atoms on the central metal atoms of C-N based SACs. For example, in 2018, Wang et al. reported the change of the electronic structure of Fe-N_4/CN SACs by one coordinated chlorine through a thermal-migrating method [55]. The obtained Fe-Cl_1N_4/CN SACs exhibited an exceptionally outstanding ORR activity compared to Fe-N_4/CN without coordinated chlorine (Figs. 9(a)–9(c)). By post-sintering strategy, five-coordinated C_1-Pt-Cl_4 SACs could be transferred to four-coordinated C_2-Pt-Cl_2 SACs for optimized electrocatalytic hydrogen evolution, as reported by Si et al. using graphdiyne as supports [58].

Support materials with modified doping or ligands could also be applied to adjust the dual-atom coordination. Elam et al. reported that the modified surface chlorine on TiO_2 could facilitate the deposition of an atomic layer of Pd, which exhibited promising performance in the low-temperature water-gas-shift reaction [115]. Yang et al. also reported that the CeF_3 clusters could further be deposited on Fe SA/CN supports, which enabled the surface chemical state to redistribute [116]. The demonstrated CeF_3-Fe SA/CN SACs exhibited enhanced electrocatalytic performance in proton exchange membrane fuel cells. Besides the dual atom coordination, SACs with dual metal sites, including Fe-Co/CN [117], Zn-Co/CN [118], Pt-Ru/CN [119], Co-Pt/CN [106], Co-Fe/CN [120], Ir-Zn/ZnO [121] and Co-Ni/CN [122], etc. were also reported to mediate their catalytic performance, which could provide with new opportunities for further development of SACs.

3.3 The second- and higher-coordination shell

Compared to the aforementioned coordination of first-shell atoms, the second- and higher-shell atoms could also influence the catalytic abilities of central metal atoms. Different from the direct coordinating atoms, atoms from the second-shell exhibited less coordinated strength, but they exhibited a moderate influence on their catalytic abilities. For example, Zhang et al. reported the synthesis of low valence Cu^+-N_4-C_8S_2 SACs, which was investigated by EXAFS together with DFT calculation (Figs. 9(f)–9(h)) [38]. Compared to S free Cu-N_4/CN SACs,

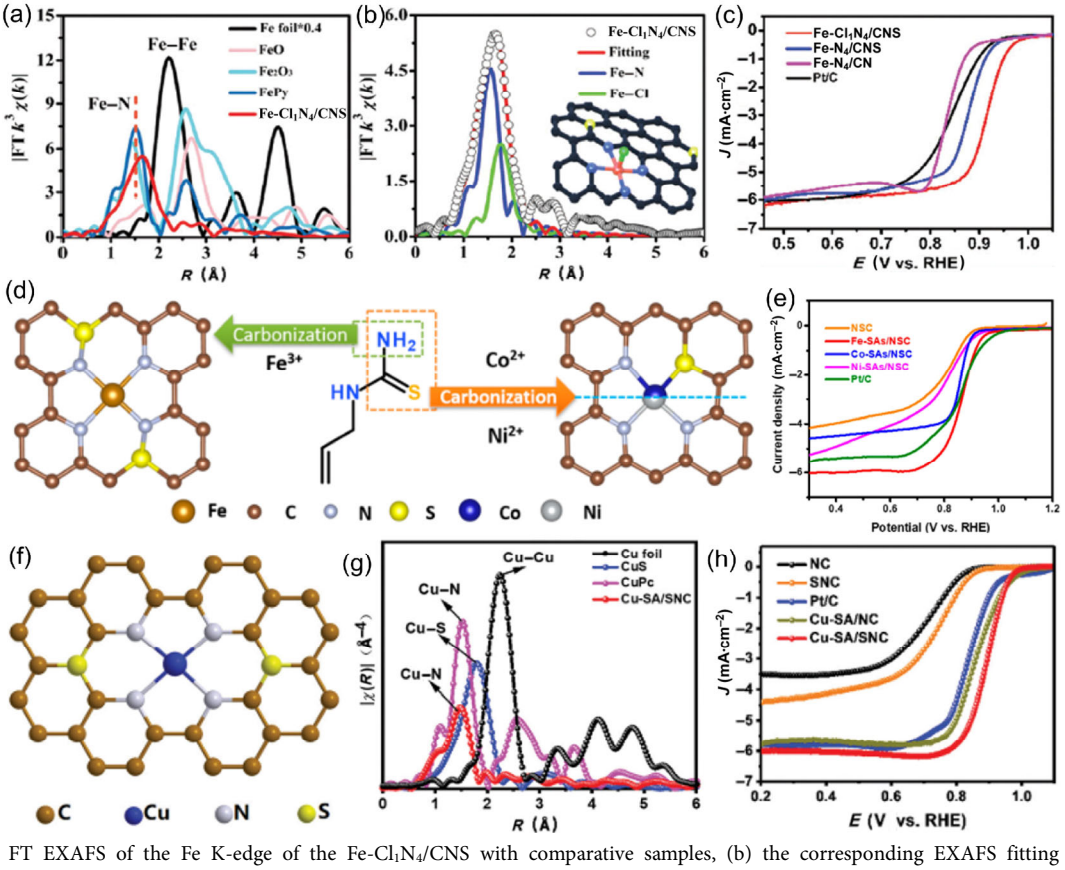

Figure 9 (a) FT EXAFS of the Fe K-edge of the Fe-Cl_1N_4/CNS with comparative samples, (b) the corresponding EXAFS fitting curves of the Fe-Cl_1N_4/CNS in *R* space with inset of schematic structure of Fe-Cl_1N_4/CNS: Fe (red), Cl (green), S (yellow), N (blue), and C (gray) and (c) corresponding ORR polarization curves in O_2 saturated 0.1 M KOH (reproduced with permission from Ref. [55], © The Royal Society of Chemistry 2019). (d) and (e) Schematic illustrations of the synthesis of Fe-N_4-C_8S_2, Ni-N_3S_1 and Co-N_3S_1, and their corresponding ORR polarization curves (reproduced with permission from Ref. [39], © American Chemical Society 2019). (f) Schematic illustration of the coordination environment, (g) FT k^3-weighted Cu K-edge EXAFS spectra and (h) corresponding ORR polarization curves of Cu-N_4-C_8S_2 (reproduced with permission from Ref. [38], © The Royal Society of Chemistry 2019).

the Cu^{+}-N_4-C_8S_2 SACs exhibited improved ORR performance in alkaline media. Similarly, Chen et al. reported Fe-S/CN SACs with enhanced ORR performance compared to S free Fe-N_4/CN SACs [55, 123]. Lee et al. also systematically investigated the controlling of the electron-withdrawing/donating properties of Fe-N_4/CN SACs by further tailoring S second-shell coordination to achieve comprehensive ORR catalytic properties [124]. Besides, in a recent study reported by Wang et al., different central metal atoms might exhibit different trends in forming a complex within an N, S-containing precursor [39]. They presented that by applying 1-allyl-2-thiourea as the precursor, Fe-N_4/C_8S_2 SACs could be achieved while Ni-N_3S_1 and Co-N_3S_1 were prepared by the same conditions (Figs. 9(d) and 9(e)). Fe-N_4/C_8S_2 exhibited better ORR performance due to the formation of a different catalytically active structure without the metal–S bonds.

Besides the S coordination, P also could work as the second-shell coordination atom. For example, Lu et al. reported the enhanced catalytic performance on hydrogenation activity of Pt-O_4-P/CeO_2 compared to Pt-O_4/CeO_2 [79]. The P doping in CeO_2 support induced a considerable charge transfer from Pt to P, which featured a significant higher valence state of Pt^{+} in Pt-O_4-P/CeO_2. To further investigate the higher-shell coordination environment, Wang et al. reported the synthesis of Fe SACs embedded on a nitrogen, phosphorus, and sulfur co-doped hollow carbon polyhedron from a metal-organic framework-polymer composite [125]. The as-prepared Fe-N_4-P-S/CN SACs exhibited remarkable performance for ORR in both alkaline and acid media, compared to Fe-N_4/CN and commercial Pt/C. The complex coordination environment provided new opportunities for developing new SACs with enhanced catalytic performance.

4 Conclusions and perspectives

The development of SACs is remarkable in recent years, and the emphasis on the coordination environment of SACs provided new opportunities for further improvement of their catalytic properties. In this review, we first discussed the characterizations of the coordination environment, mainly concerning X-ray derived techniques, *in situ* techniques, and theoretical predictions, which are important for the determination of the coordination environment. Then, categorized by support materials and coordination atoms, the local coordination environments of recently reported SACs were systematically discussed, especially concerning the modulating of the coordination environments of central metal atoms and their corresponding influence on catalytic properties. The study on the coordination environment of SACs could help researchers to deeply investigate the structure evolution and working mechanism during the catalytic process. The current progress of enhanced catalytic performance facilitated by tailoring the coordination atoms, coordination number, and second- or higher-coordination shells confirms the great significance and opportunities of their applications. Opportunities and challenges still exist to modulate the coordination environments further and optimize the catalytic properties of SACs.

(1) The detailed characterizations of the coordination environment of SACs are still not satisfactory for complicated cases, such as dual-metal sites SACs and multi-shell coordinated SACs. As mentioned in Section 2, such complicated coordination is mainly determined by the comprehensive consideration of experimental spectra and theoretical predictions. More convincing characterized strategies could be helpful in a further determination of complicated coordination environment. To date, some specific coordination on specific supports (mainly 2D transition-metal dichalcogenides) could be directly observed by annular dark-field STEM or aberration-corrected STEM, characterizations for general support materials are still restrained due to technical limitations.

(2) To date, the characterizations of coordination environments and related charge transfer during the catalytic process were mainly dependent on theoretical modelings. How to provide direct observations of the dynamic changes during the catalytic process is an attractive challenge. New *in situ* technologies such as *in situ* scanning tunneling microscopy and *in situ* aberration-corrected STEM could be helpful for the understanding of catalytic mechanisms and further theoretical studies.

(3) New SACs with precisely designed coordination environments might exhibit novel catalytic performance. As mentioned in previous sections, the coordination atoms could significantly influence the electronic and geometric structures of central metal atoms. Though SACs exhibited high catalytic performance in many reactions, further improvement by coordination tailoring could be effective and applicable. For example, additional coordination of center atoms by some specific element at higher shells (such as S, Se, P, etc.) might increase the stability of SACs without loss of catalytic activity. A slightly mediated coordination of center atoms could increase the dynamic activity, which might increase the catalytic activity and meanwhile maintained high stability due to the structure flexibility.

(4) The strategies on modulating the coordination environments of SACs could provide new opportunities to synthesize SACs on a large scale. For example, metal nanoparticles anchored on various support could be transformed to SACs due to the coordination environment by easily performed mechanical treatment as reported by many leading groups on SACs. Meanwhile, most of the heterogeneous catalysts consisted of bulk or nano-scale metal materials. Hence, post-treatment of existing heterogeneous catalysts could be an appropriate strategy for large scale synthesis of SACs for industrial applications.

Acknowledgements

This work was supported by the National Key R&D Program of China (Nos. 2018YFA0702003 and 2016YFA0202801), the National Natural Science Foundation of China (Nos. 51631001, 51872030, 21890383, 21671117, 21871159, 21901135, 51702016, and 51501010), Beijing Institute of Technology Research Fund Program for Young Scholars, and Beijing Municipal Science & Technology Commission (No. Z191100007219003).

References

[1] Chen, Y. J.; Ji, S. F.; Chen, C.; Peng, Q.; Wang, D. S.; Li, Y. D. Single-atom catalysts: Synthetic strategies and electrochemical applications. *Joule* **2018**, *2*, 1242–1264.

[2] Yang, X. F.; Wang, A. Q.; Qiao, B. T.; Li, J.; Liu, J. Y.; Zhang, T. Single-atom catalysts: A new frontier in heterogeneous catalysis. *Acc. Chem. Res.* **2013**, *46*, 1740–1748.

[3] Jia, Y.; Jiang, K.; Wang, H. T.; Yao, X. D. The role of defect sites in nanomaterials for electrocatalytic energy conversion. *Chem* **2019**, *5*, 1371–1397.

[4] Cook, S. A.; Borovik, A. S. Molecular designs for controlling the local environments around metal ions. *Acc. Chem. Res.* **2015**, *48*, 2407–2414.

[5] Tao, L.; Wang, Y. Q.; Zou, Y. Q.; Zhang, N.; Zhang, Y. Q.; Wu, Y. J.; Wang, Y. Y.; Chen, R.; Wang, S. Y. Charge transfer modulated activity of carbon-based electrocatalysts. *Adv. Energy Mater.* **2020**, *10*, 1901227.

[6] Sun, T. T.; Xu, L. B.; Wang, D. S.; Li, Y. D. Metal organic frameworks derived single atom catalysts for electrocatalytic energy conversion.

Nano Res. **2019**, *12*, 2067–2080.
[7] Mao, J. J.; Li, J.; Pei, J. J.; Liu, Y.; Wang, D. S.; Li, Y. D. Structure regulation of noble-metal-based nanomaterials at an atomic level. *Nano Today* **2019**, *26*, 164–175.
[8] Wen, J. F.; Chen, Y. J.; Ji, S. F.; Zhang, J.; Wang, D. S.; Li, Y. D. Metal-organic frameworks-derived nitrogen-doped carbon supported nanostructured PtNi catalyst for enhanced hydrosilylation of 1-octene. *Nano Res.* **2019**, *12*, 2584–2588.
[9] Qiao, B. T.; Wang, A. Q.; Yang, X. F.; Allard, L. F.; Jiang, Z.; Cui, Y. T.; Liu, J. Y.; Li, J.; Zhang, T. Single-atom catalysis of CO oxidation using Pt_1/FeO_x. *Nat. Chem.* **2011**, *3*, 634–641.
[10] Li, Z. J.; Wang, D. H.; Wu, Y.; Li, Y. D. Recent advances in the precise control of isolated single-site catalysts by chemical methods. *Natl. Sci. Rev.* **2018**, *5*, 673–689.
[11] Deng, D. H.; Chen, X. Q.; Yu, L.; Wu, X.; Liu, Q. F.; Liu, Y.; Yang, H. X.; Tian, H. F.; Hu, Y. F.; Du, P. P. et al. A single iron site confined in a graphene matrix for the catalytic oxidation of benzene at room temperature. *Sci. Adv.* **2015**, *1*, e1500462.
[12] Deng, J.; Li, H. B.; Xiao, J. P.; Tu, Y. C.; Deng, D. H.; Yang, H. X.; Tian, H. F.; Li, J. Q.; Ren, P. J.; Bao, X. H. Triggering the electrocatalytic hydrogen evolution activity of the inert two-dimensional MoS_2 surface via single-atom metal doping. *Energy Environ. Sci.* **2015**, *8*, 1594–1601.
[13] Liu, J. Y. Catalysis by supported single metal atoms. *ACS Catal.* **2017**, *7*, 34–59.
[14] Lin, J.; Wang, X. D. Rh single atom catalyst for direct conversion of methane to oxygenates. *Sci. China Mater.* **2018**, *61*, 758–760.
[15] Lang, R.; Xi, W.; Liu, J. C.; Cui, Y. T.; Li, T. B.; Lee, A. F.; Chen, F.; Chen, Y.; Li, L.; Li, L. et al. Non defect-stabilized thermally stable single-atom catalyst. *Nat. Commun.* **2019**, *10*, 234.
[16] Liang, Z. B.; Guo, W. H.; Zhao, R.; Qiu, T. J.; Tabassum, H.; Zou, R. Q. Engineering atomically dispersed metal sites for electrocatalytic energy conversion. *Nano Energy* **2019**, *64*, 103917.
[17] Liu, J.; Jin, Z.; Wang, X.; Ge, J. J.; Liu, C. P.; Xing, W. Recent advances in active sites identification and regulation of M-N/C electro-catalysts towards ORR. *Sci. China Chem.* **2019**, *62*, 669–683.
[18] Qiao, B. T.; Liang, J. X.; Wang, A. Q.; Xu, C. Q.; Li, J.; Zhang, T.; Liu, J. J. Ultrastable single-atom gold catalysts with strong covalent metal–support interaction (CMSI). *Nano Res.* **2015**, *8*, 2913–2924.
[19] Sun, G. D.; Zhao, Z. J.; Mu, R. T.; Zha, S. J.; Li, L. L.; Chen, S.; Zang, K. T.; Luo, J.; Li, Z. L.; Purdy, S. C. et al. Breaking the scaling relationship via thermally stable Pt/Cu single atom alloys for catalytic dehydrogenation. *Nat. Commun.* **2018**, *9*, 4454.
[20] Marcinkowski, M. D.; Darby, M. T.; Liu, J. L.; Wimble, J. M.; Lucci, F. R.; Lee, S.; Michaelides, A.; Flytzani-Stephanopoulos, M.; Stamatakis, M.; Sykes, E. C. H. Pt/Cu single-atom alloys as coke-resistant catalysts for efficient C–H activation. *Nat. Chem.* **2018**, *10*, 325–332.
[21] Liu, W. G.; Zhang, L. L.; Liu, X.; Liu, X. Y.; Yang, X. F.; Miao, S.; Wang, W. T.; Wang, A. Q.; Zhang, T. Discriminating catalytically active FeN_x species of atomically dispersed Fe–N–C catalyst for selective oxidation of the C–H bond. *J. Am. Chem. Soc.* **2017**, *139*, 10790–10798.
[22] Liu, M. M.; Wang, L. L.; Zhao, K. N.; Shi, S. S.; Shao, Q. S.; Zhang, L.; Sun, X. L.; Zhao, Y. F.; Zhang, J. J. Atomically dispersed metal catalysts for the oxygen reduction reaction: Synthesis, characterization, reaction mechanisms and electrochemical energy applications. *Energy Environ. Sci.* **2019**, *12*, 2890–2923.
[23] Wang, X. Q.; Li, Z. J.; Qu, Y. T.; Yuan, T. W.; Wang, W. Y.; Wu, Y. E.; Li, Y. D. Review of metal catalysts for oxygen reduction reaction: From nanoscale engineering to atomic design. *Chem* **2019**, *5*, 1486–1511.
[24] Tao, H. C.; Choi, C.; Ding, L. X.; Jiang, Z.; Han, Z. S.; Jia, M. W.; Fan, Q.; Gao, Y. N.; Wang, H. H.; Robertson, A. W. et al. Nitrogen fixation by Ru single-atom electrocatalytic reduction. *Chem* **2019**, *5*, 204–214.
[25] Liu, X.; Jiao, Y.; Zheng, Y.; Jaroniec, M.; Qiao, S. Z. Building up a picture of the electrocatalytic nitrogen reduction activity of transition metal single-atom catalysts. *J. Am. Chem. Soc.* **2019**, *141*, 9664–9672.
[26] Zhao, C. M.; Wang, Y.; Li, Z. J.; Chen, W. X.; Xu, Q.; He, D. S.; Xi, D. S.; Zhang, Q. H.; Yuan, T. W.; Qu, Y. T. et al. Solid-diffusion synthesis of single-atom catalysts directly from bulk metal for efficient CO_2 reduction. *Joule* **2019**, *3*, 584–594.
[27] Millet, M. M.; Algara-Siller, G.; Wrabetz, S.; Mazheika, A.; Girgsdies, F.; Teschner, D.; Seitz, F.; Tarasov, A.; Levchenko, S. V.; Schlögl, R. et al. Ni single atom catalysts for CO_2 activation. *J. Am. Chem. Soc.* **2019**, *141*, 2451–2461.
[28] Jiao, J. Q.; Lin, R.; Liu, S. J.; Cheong, W. C.; Zhang, C.; Chen, Z.; Pan, Y.; Tang, J. G.; Wu, K. L.; Hung, S. F. et al. Copper atom-pair catalyst anchored on alloy nanowires for selective and efficient electrochemical reduction of CO_2. *Nat. Chem.* **2019**, *11*, 222–228.
[29] Zhang, Z.; Ma, C.; Tu, Y. C.; Si, R.; Wei, J.; Zhang, S. H.; Wang, Z.; Li, J. F.; Wang, Y.; Deng, D. H. Multiscale carbon foam confining single iron atoms for efficient electrocatalytic CO_2 reduction to CO. *Nano Res.* **2019**, *12*, 2313–2317.
[30] Liu, P. X.; Zheng, N. F. Coordination chemistry of atomically dispersed catalysts. *Natl. Sci. Rev.* **2018**, *5*, 636–638.
[31] Liu, J. C.; Tang, Y.; Wang, Y. G.; Zhang, T.; Li, J. Theoretical understanding of the stability of single-atom catalysts. *Natl. Sci. Rev.* **2018**, *5*, 638–641.
[32] Zhu, Y. Z.; Peng, W. C.; Li, Y.; Zhang, G. L.; Zhang, F. B.; Fan, X. B. Modulating the electronic structure of single-atom catalysts on 2D nanomaterials for enhanced electrocatalytic performance. *Small Methods* **2019**, *3*, 1800438.
[33] Wang, Y.; Chen, Z.; Shen, R.; Cao, X.; Chen, Y. G.; Chen, C.; Wang, D. S.; Peng, Q.; Li, Y. D. Pd-dispersed CuS hetero-nanoplates for selective hydrogenation of phenylacetylene. *Nano Res.* **2016**, *9*, 1209–1219.
[34] Liang, J. X.; Yu, Q.; Yang, X. F.; Zhang, T.; Li, J. A systematic theoretical study on FeO_x-supported single-atom catalysts: M_1/FeO_x for CO oxidation. *Nano Res.* **2018**, *11*, 1599–1611.
[35] Gui, J.; Ji, M. W.; Liu, J. J.; Xu, M.; Zhang, J. T.; Zhu, H. S. Phosphine-initiated cation exchange for precisely tailoring composition and properties of semiconductor nanostructures: Old concept, new applications. *Angew. Chem., Int. Ed.* **2015**, *54*, 3683–3687.
[36] Bai, B.; Xu, M.; Li, N.; Chen, W. X.; Liu, J. J.; Liu, J.; Rong, H. P.; Fenske, D.; Zhang, J. T. Semiconductor nanocrystal engineering by applying thiol- and solvent-coordinated cation exchange kinetics. *Angew. Chem., Int. Ed.* **2019**, *58*, 4852–4857.
[37] Li, X. Y.; Iqbal, M. A.; Xu, M.; Wang, Y. C.; Wang, H. Z.; Ji, M. W.; Wan, X. D.; Slater, T. J. A.; Liu, J.; Liu, J. J. et al. $Au@Hg_xCd_{1-x}Te$ core@shell nanorods by sequential aqueous cation exchange for near-infrared photodetectors. *Nano Energy* **2019**, *57*, 57–65.
[38] Jiang, Z. L.; Sun, W. M.; Shang, H. S.; Chen, W. X.; Sun, T. T.; Li, H. J.; Dong, J. C.; Zhou, J.; Li, Z.; Wang, Y. et al. Atomic interface effect of a single atom copper catalyst for enhanced oxygen reduction reactions. *Energy Environ. Sci.* **2019**, *12*, 3508–3514.
[39] Zhang, J. Q.; Zhao, Y. F.; Chen, C.; Huang, Y. C.; Dong, C. L.; Chen, C. J.; Liu, R. S.; Wang, C. Y.; Yan, K.; Li, Y. D. et al. Tuning the coordination environment in single-atom catalysts to achieve highly efficient oxygen reduction reactions. *J. Am. Chem. Soc.* **2019**, *141*, 20118–20126.
[40] Chen, W. X.; Pei, J. J.; He, C. T.; Wan, J. W.; Ren, H. L.; Wang, Y.; Dong, J. C.; Wu, K. L.; Cheong, W. C.; Mao, J. J. et al. Single tungsten atoms supported on MOF-derived N-doped carbon for robust electrochemical hydrogen evolution. *Adv. Mater.* **2018**, *30*, 1800396.
[41] Li, Z.; Ji, S. F.; Liu, Y. W.; Cao, X.; Tian, S. B.; Chen, Y. J.; Niu, Z. Q.; Li, Y. D. Well-defined materials for heterogeneous catalysis: From nanoparticles to isolated single-atom sites. *Chem. Rev.* **2020**, *120*, 623−682.
[42] Bordiga, S.; Groppo, E.; Agostini, G.; van Bokhoven, J. A.; Lamberti, C. Reactivity of surface species in heterogeneous catalysts probed by *in situ* X-ray absorption techniques. *Chem. Rev.* **2013**, *113*, 1736–1850.
[43] Moliner, M.; Gabay, J. E.; Kliewer, C. E.; Carr, R. T.; Guzman, J.; Casty, G. L.; Serna, P.; Corma, A. Reversible transformation of Pt nanoparticles into single atoms inside high-silica chabazite zeolite. *J. Am. Chem. Soc.* **2016**, *138*, 15743−15750.
[44] Becknell, N.; Kang, Y. J.; Chen, C.; Resasco, J.; Kornienko, N.; Guo, J. H.; Markovic, N. M.; Somorjai, G. A.; Stamenkovic, V. R.; Yang, P. D. Atomic structure of Pt_3Ni nanoframe electrocatalysts by *in situ* X−ray absorption spectroscopy. *J. Am. Chem. Soc.* **2015**, *137*, 15817–15824.
[45] Xiao, M. L.; Zhu, J. B.; Ma, L.; Jin, Z.; Ge, J. J.; Deng, X.; Hou, Y.; He, Q. G.; Li, J. K.; Jia, Q. Y. et al. Microporous framework induced

synthesis of single-atom dispersed Fe-N-C acidic ORR catalyst and its *in situ* reduced Fe-N_4 active site identification revealed by X-ray absorption spectroscopy. *ACS Catal.* **2018**, *8*, 2824–2832.

[46] Wang, L. B.; Zhang, W. B.; Wang, S. P.; Gao, Z. H.; Luo, Z. H.; Wang, X.; Zeng, R.; Li, A. W.; Li, H. L.; Wang, M. L. et al. Atomic-level insights in optimizing reaction paths for hydroformylation reaction over Rh/CoO single-atom catalyst. *Nat. Commun.* **2016**, *7*, 14036.

[47] Zhang, E. H.; Wang, T.; Yu, K.; Liu, J.; Chen, W. X.; Li, A.; Rong, H. P.; Lin, R.; Ji, S. F.; Zheng, X. S. et al. Bismuth single atoms resulting from transformation of metal–organic frameworks and their use as electrocatalysts for CO_2 reduction. *J. Am. Chem. Soc.* **2019**, *141*, 16569–16573.

[48] Matsubu, J. C.; Zhang, S. Y.; DeRita, L.; Marinkovic, N. S.; Chen, J. G.; Graham, G. W.; Pan, X. Q.; Christopher, P. Adsorbate-mediated strong metal–support interactions in oxide-supported Rh catalysts. *Nat. Chem.* **2017**, *9*, 120–127.

[49] Lin, Y. C.; Dumcenco, D. O.; Komsa, H. P.; Niimi, Y.; Krasheninnikov, A. V.; Huang, Y. S.; Suenaga, K. Properties of individual dopant atoms in single-layer MoS_2: Atomic structure, migration, and enhanced reactivity. *Adv. Mater.* **2014**, *26*, 2857–2861.

[50] DeRita, L.; Resasco, J.; Dai, S.; Boubnov, A.; Thang, H. V.; Hoffman, A. S.; Ro, I.; Graham, G. W.; Bare, S. R.; Pacchioni, G. et al. Structural evolution of atomically dispersed Pt catalysts dictates reactivity. *Nat. Mater.* **2019**, *18*, 746–751.

[51] Xu, H. X.; Cheng, D. J.; Cao, D. P.; Zeng, X. C. A universal principle for a rational design of single-atom electrocatalysts. *Nat. Catal.* **2018**, *1*, 339–348.

[52] Zhu, G. Q.; Liu, F.; Wang, Y. C.; Wei, Z. D.; Wang, W. Systematic exploration of N, C coordination effects on the ORR performance of Mn–N_x doped graphene catalysts based on DFT calculations. *Phys. Chem. Chem. Phys.* **2019**, *21*, 12826–12836.

[53] Wan, C. Z.; Duan, X. F.; Huang, Y. Molecular design of single-atom catalysts for oxygen reduction reaction. *Adv. Energy Mater.*, in press, DOI: 10.1002/aenm.201903815.

[54] Zitolo, A.; Goellner, V.; Armel, V.; Sougrati, M. T.; Mineva, T.; Stievano, L.; Fonda, E.; Jaouen, F. Identification of catalytic sites for oxygen reduction in iron- and nitrogen-doped graphene materials. *Nat. Mater.* **2015**, *14*, 937–942.

[55] Han, Y. H.; Wang, Y. G.; Xu, R. R.; Chen, W. X.; Zheng, L. R.; Han, A. J.; Zhu, Y. Q.; Zhang, J.; Zhang, H. B.; Luo, J. et al. Electronic structure engineering to boost oxygen reduction activity by controlling the coordination of the central metal. *Energy Environ. Sci.* **2018**, *11*, 2348–2352.

[56] Qiu, H. J.; Ito, Y.; Cong, W. T.; Tan, Y. W.; Liu, P.; Hirata, A.; Fujita, T.; Tang, Z.; Chen, M. W. Nanoporous graphene with single-atom nickel dopants: An efficient and stable catalyst for electrochemical hydrogen production. *Angew. Chem., Int. Ed.* **2015**, *54*, 14031–14035.

[57] Yan, H.; Cheng, H.; Yi, H.; Lin, Y.; Yao, T.; Wang, C. L.; Li, J. J.; Wei, S. Q.; Lu, J. L. Single-atom Pd_1/graphene catalyst achieved by atomic layer deposition: Remarkable performance in selective hydrogenation of 1,3-butadiene. *J. Am. Chem. Soc.* **2015**, *137*, 10484–10487.

[58] Yin, X. P.; Wang, H. J.; Tang, S. F.; Lu, X. L.; Shu, M.; Si, R.; Lu, T. B. Engineering the coordination environment of single-atom platinum anchored on graphdiyne for optimizing electrocatalytic hydrogen evolution. *Angew. Chem., Int. Ed.* **2018**, *57*, 9382–9386.

[59] Zhu, Y. Q.; Sun, W. M.; Luo, J.; Chen, W. X.; Cao, T.; Zheng, L. R.; Dong, J. C.; Zhang, J.; Zhang, M. L.; Han, Y. H. et al. A cocoon silk chemistry strategy to ultrathin N-doped carbon nanosheet with metal single-site catalysts. *Nat. Commun.* **2018**, *9*, 3861.

[60] Li, H. N.; Cao, C. Y.; Liu, J.; Shi, Y.; Si, R.; Gu, L.; Song, W. G. Cobalt single atoms anchored on N-doped ultrathin carbon nanosheets for selective transfer hydrogenation of nitroarenes. *Sci. China Mater.* **2019**, *62*, 1306–1314.

[61] Zhou, S. Q.; Shang, L.; Zhao, Y. X.; Shi, R.; Waterhouse, G. I. N.; Huang, Y. C.; Zheng, L. R.; Zhang, T. R. Pd single-atom catalysts on nitrogen-doped graphene for the highly selective photothermal hydrogenation of acetylene to ethylene. *Adv. Mater.* **2019**, *31*, 1900509.

[62] Jiang, K.; Siahrostami, S.; Zheng, T. T.; Hu, Y. F.; Hwang, S.; Stavitski, E.; Peng, Y. D.; Dynes, J.; Gangisetty, M.; Su, D. et al. Isolated Ni single atoms in graphene nanosheets for high-performance CO_2 reduction. *Energy Environ. Sci.* **2018**, *11*, 893–903.

[63] Peng, P.; Shi, L.; Huo, F.; Mi, C. X.; Wu, X. H.; Zhang, S. J.; Xiang, Z. H. A pyrolysis-free path toward superiorly catalytic nitrogen-coordinated single atom. *Sci. Adv.* **2019**, *5*, eaaw2322.

[64] Yin, P. Q.; Yao, T.; Wu, Y.; Zheng, L. R.; Lin, Y.; Liu, W.; Ju, H. X.; Zhu, J. F.; Hong, X.; Deng, Z. X. et al. Single cobalt atoms with precise N-coordination as superior oxygen reduction reaction catalysts. *Angew. Chem., Int. Ed.* **2016**, *55*, 10800–10805.

[65] Wang, X. X.; Cullen, D. A.; Pan, Y. T.; Hwang, S.; Wang, M. Y.; Feng, Z. X.; Wang, J. Y.; Engelhard, M. H.; Zhang, H. G.; He, Y. H. et al. Nitrogen-coordinated single cobalt atom catalysts for oxygen reduction in proton exchange membrane fuel cells. *Adv. Mater.* **2018**, *30*, 1706758.

[66] Ji, S. F.; Chen, Y. J.; Zhao, S.; Chen, W. X.; Shi, L. J.; Wang, Y.; Dong, J. C.; Li, Z.; Li, F. W.; Chen, C. et al. Atomically dispersed ruthenium species inside metal–organic frameworks: Combining the high activity of atomic sites and the molecular sieving effect of MOFs. *Angew. Chem., Int. Ed.* **2019**, *131*, 4315–4319.

[67] Zhao, C. M.; Dai, X. Y.; Yao, T.; Chen, W. X.; Wang, X. Q.; Wang, J.; Yang, J.; Wei, S. Q.; Wu, Y.; Li, Y. D. Ionic exchange of metal–organic frameworks to access single nickel sites for efficient electroreduction of CO_2. *J. Am. Chem. Soc.* **2017**, *139*, 8078–8081.

[68] Han, Y. H.; Wang, Y. G.; Chen, W. X.; Xu, R. R.; Zheng, L. R.; Zhang, J.; Luo, J.; Shen, R. A.; Zhu, Y. Q.; Cheong, W. C. et al. Hollow N-doped carbon spheres with isolated cobalt single atomic sites: Superior electrocatalysts for oxygen reduction. *J. Am. Chem. Soc.* **2017**, *139*, 17269–17272.

[69] Zhang, M. L.; Wang, Y. G.; Chen, W. X.; Dong, J. C.; Zheng, L. R.; Luo, J.; Wan, J. W.; Tian, S. B.; Cheong, W. C.; Wang, D. S. et al. Metal (hydr)oxides@polymer core–shell strategy to metal single-atom materials. *J. Am. Chem. Soc.* **2017**, *139*, 10976–10979.

[70] Zhang, L. Z.; Jia, Y.; Liu, H. L.; Zhuang, L. Z.; Yan, X. C.; Lang, C. G.; Wang, X.; Yang, D. J.; Huang, K. K.; Feng, S. H. et al. Charge polarization from atomic metals on adjacent graphitic layers for enhancing the hydrogen evolution reaction. *Angew. Chem., Int. Ed.* **2019**, *58*, 9404–9408.

[71] Lin, J.; Wang, A. Q.; Qiao, B. T.; Liu, X. Y.; Yang, X. F.; Wang, X. D.; Liang, J. X.; Li, J.; Liu, J. Y.; Zhang, T. Remarkable performance of Ir_1/FeO_x single-atom catalyst in water gas shift reaction. *J. Am. Chem. Soc.* **2013**, *135*, 15314–15317.

[72] Liu, P. X.; Zhao, Y.; Qin, R. X.; Mo, S. G.; Chen, G. X.; Gu, L.; Chevrier, D. M.; Zhang, P.; Guo, Q.; Zang, D. D. et al. Photochemical route for synthesizing atomically dispersed palladium catalysts. *Science* **2016**, *352*, 797–801.

[73] Wan, J. W.; Chen, W. X.; Jia, C. Y.; Zheng, L. R.; Dong, J. C.; Zheng, X. S.; Wang, Y.; Yan, W. S.; Chen, C.; Peng, Q. et al. Defect effects on TiO_2 nanosheets: Stabilizing single atomic site Au and promoting catalytic properties. *Adv. Mater.* **2018**, *30*, 1705369.

[74] Chen, Y. J.; Ji, S. F.; Sun, W. M.; Chen, W. X.; Dong, J. C.; Wen, J. F.; Zhang, J.; Li, Z.; Zheng, L. R.; Chen, C. et al. Discovering partially charged single-atom Pt for enhanced anti-Markovnikov alkene hydrosilylation. *J. Am. Chem. Soc.* **2018**, *140*, 7407–7410.

[75] Chen, Y. J.; Ji, S. F.; Sun, W. M.; Lei, Y. P.; Wang, Q. C.; Li, A.; Chen, W. X.; Zhou, G.; Zhang, Z. D.; Wang, Y. et al. Engineering the atomic interface with single platinum atoms for enhanced photocatalytic hydrogen production. *Angew. Chem., Int. Ed.* **2020**, *59*, 1295–1301.

[76] Tang, Y.; Asokan, C.; Xu, M. J.; Graham, G. W.; Pan, X. Q.; Christopher, P.; Li, J.; Sautet, P. Rh single atoms on TiO_2 dynamically respond to reaction conditions by adapting their site. *Nat. Commun.* **2019**, *10*, 4488.

[77] Ren, Y. J.; Tang, Y.; Zhang, L. L.; Liu, X. Y.; Li, L.; Miao, S.; Sheng Su, D.; Wang, A. Q.; Li, J.; Zhang, T. Unraveling the coordination structure-performance relationship in Pt_1/Fe_2O_3 single-atom catalyst. *Nat. Commun.* **2019**, *10*, 4500.

[78] Park, J.; Lee, S.; Kim, H. E.; Cho, A.; Kim, S.; Ye, Y. J.; Han, J. W.; Lee, H.; Jang, J. H.; Lee, J. Investigation of the support effect in atomically dispersed Pt on WO_{3-x} for utilization of Pt in the hydrogen evolution reaction. *Angew. Chem., Int. Ed.* **2019**, *58*, 16038–16042.

[79] Ma, Y. F.; Chi, B. L.; Liu, W.; Cao, L.; Lin, Y.; Zhang, X. H.; Ye, X. X.; Wei, S. Q.; Lu, J. L. Tailoring of the proximity of platinum single atoms on CeO_2 using phosphorus boosts the hydrogenation activity. *ACS Catal.* **2019**, *9*, 8404–8412.

[80] Ye, X. X.; Wang, H. W.; Lin, Y.; Liu, X. Y.; Cao, L.; Gu, J.; Lu, J. L. Insight of the stability and activity of platinum single atoms on ceria.

Nano Res. **2019**, *12*, 1401–1409.
[81] Chen, F.; Li, T. B.; Pan, X. L.; Guo, Y. L.; Han, B.; Liu, F.; Qiao, B. T.; Wang, A. Q.; Zhang, T. Pd_1/CeO_2 single-atom catalyst for alkoxycarbonylation of aryl iodides. *Sci. China Mater.*, in press, DOI: 10.1007/s40843-019-1204-y.
[82] Liu, K. L.; Qin, R. X.; Zhou, L. Y.; Liu, P. X.; Zhang, Q. H.; Jing, W. T.; Ruan, P. P.; Gu, L.; Fu, G.; Zheng, N. F. Cu_2O-supported atomically dispersed Pd catalysts for semihydrogenation of terminal alkynes: Critical role of oxide supports. *CCS Chem.* **2019**, *1*, 207–214.
[83] Zhou, X.; Shen, Q.; Yuan, K. D.; Yang, W. S.; Chen, Q. W.; Geng, Z. H.; Zhang, J. L.; Shao, X.; Chen, W.; Xu, G. Q. et al. Unraveling charge State of supported Au single-atoms during CO oxidation. *J. Am. Chem. Soc.* **2018**, *140*, 554–557.
[84] Li, J. J.; Guan, Q. Q.; Wu, H.; Liu, W.; Lin, Y.; Sun, Z. H.; Ye, X. X.; Zheng, X. S.; Pan, H. B.; Zhu, J. F. et al. Highly active and stable metal single-atom catalysts achieved by strong electronic metal–support interactions. *J. Am. Chem. Soc.* **2019**, *141*, 14515–14519.
[85] Zhang, J.; Wu, X.; Cheong, W. C.; Chen, W. X.; Lin, R.; Li, J.; Zheng, L. R.; Yan, W. S.; Gu, L.; Chen, C. et al. Cation vacancy stabilization of single-atomic-site $Pt_1/Ni(OH)_x$ catalyst for diboration of alkynes and alkenes. *Nat. Commun.* **2018**, *9*, 1002.
[86] Wang, F. F.; Li, Q.; Xu, D. S. Recent progress in semiconductor-based nanocomposite photocatalysts for solar-to-chemical energy conversion. *Adv. Energy Mater.* **2017**, *7*, 1700529.
[87] Chandrasekaran, S.; Yao, L.; Deng, L. B.; Bowen, C.; Zhang, Y.; Chen, S. M.; Lin, Z. Q.; Peng, F.; Zhang, P. X. Recent advances in metal sulfides: From controlled fabrication to electrocatalytic, photocatalytic and photoelectrochemical water splitting and beyond. *Chem. Soc. Rev.* **2019**, *48*, 4178–4280.
[88] Wang, B.; Cai, H. R.; Shen, S. H. Single metal atom photocatalysis. *Small Methods* **2019**, *3*, 1800447.
[89] Liu, L. C.; Corma, A. Metal catalysts for heterogeneous catalysis: From single atoms to nanoclusters and nanoparticles. *Chem. Rev.* **2018**, *118*, 4981–5079.
[90] Li, H. S.; Wang, S. S.; Sawada, H.; Han, G. G. D.; Samuels, T.; Allen, C. S.; Kirkland, A. I.; Grossman, J. C.; Warner, J. H. Atomic structure and dynamics of single platinum atom interactions with monolayer MoS_2. *ACS Nano* **2017**, *11*, 3392–3403.
[91] Liu, G. L.; Robertson, A. W.; Li, M. M. J.; Kuo, W. C. H.; Darby, M. T.; Muhieddine, M. H.; Lin, Y. C.; Suenaga, K.; Stamatakis, M.; Warner, J. H. et al. MoS_2 monolayer catalyst doped with isolated Co atoms for the hydrodeoxygenation reaction. *Nat. Chem.* **2017**, *9*, 810–816.
[92] Liu, J.; Zhao, Q.; Liu, J. L.; Wu, Y. S.; Cheng, Y.; Ji, M. W.; Qian, H. M.; Hao, W. C.; Zhang, L. J.; Wei, X. J. et al. Heterovalent-doping-enabled efficient dopant luminescence and controllable electronic impurity via a new strategy of preparing II−VI nanocrystals. *Adv. Mater.* **2015**, *27*, 2753–2761.
[93] Wang, H. Z.; Gao, Y. Y.; Liu, J.; Li, X. Y.; Ji, M. W.; Zhang, E. H.; Cheng, X. Y.; Xu, M.; Liu, J. J.; Rong, H. P. et al. Efficient plasmonic Au/CdSe nanodumbbell for photoelectrochemical hydrogen generation beyond visible region. *Adv. Energy Mater.* **2019**, *9*, 1803889.
[94] Pan, R. R.; Liu, J.; Li, Y. M.; Li, X. Y.; Zhang, E. H.; Di, Q. M.; Su, M. Y.; Zhang, J. T. Electronic doping-enabled transition from n- to p-type conductivity over Au@CdS core–shell nanocrystals toward unassisted photoelectrochemical water splitting. *J. Mater. Chem. A* **2019**, *7*, 23038–23045.
[95] Shen, R. G.; Chen, W. X.; Peng, Q.; Lu, S. Q.; Zheng, L. R.; Cao, X.; Wang, Y.; Zhu, W.; Zhang, J. T.; Zhuang, Z. B. et al. High-concentration single atomic Pt sites on hollow CuS_x for selective O_2 reduction to H_2O_2 in acid solution. *Chem* **2019**, *5*, 2099–2110.
[96] Ge, J. J.; He, D. S.; Chen, W. X.; Ju, H. X.; Zhang, H.; Chao, T. T.; Wang, X. Q.; You, R.; Lin, Y.; Wang, Y. et al. Atomically dispersed Ru on ultrathin Pd nanoribbons. *J. Am. Chem. Soc.* **2016**, *138*, 13850–13853.
[97] Zhang, H. J.; Watanabe, T.; Okumura, M.; Haruta, M.; Toshima, N. Catalytically highly active top gold atom on palladium nanocluster. *Nat. Mater.* **2012**, *11*, 49–52.
[98] Pei, G. X.; Liu, X. Y.; Wang, A. Q.; Lee, A. F.; Isaacs, M. A.; Li, L.; Pan, X. L.; Yang, X. F.; Wang, X. D.; Tai, Z. J. et al. Ag alloyed Pd single-atom catalysts for efficient selective hydrogenation of acetylene to ethylene in excess ethylene. *ACS Catal.* **2015**, *5*, 3717–3725.
[99] Mao, J. J.; He, C. T.; Pei, J. J.; Chen, W. X.; He, D. S.; He, Y. Q.; Zhuang, Z. B.; Chen, C.; Peng, Q.; Wang, D. S. et al. Accelerating water dissociation kinetics by isolating cobalt atoms into ruthenium lattice. *Nat. Commun.* **2018**, *9*, 4958.
[100] Liu, J. L.; Lucci, F. R.; Yang, M.; Lee, S.; Marcinkowski, M. D.; Therrien, A. J.; Williams, C. T.; Sykes, E. C. H.; Flytzani-Stephanopoulos, M. Tackling CO poisoning with single-atom alloy catalysts. *J. Am. Chem. Soc.* **2016**, *138*, 6396–6399.
[101] Yao, Y. C.; Hu, S. L.; Chen, W. X.; Huang, Z. Q.; Wei, W. C.; Yao, T.; Liu, R. R.; Zang, K. T.; Wang, X. Q.; Wu, G. et al. Engineering the electronic structure of single atom Ru sites via compressive strain boosts acidic water oxidation electrocatalysis. *Nat. Catal.* **2019**, *2*, 304–313.
[102] Rong, H. P.; Mao, J. J.; Xin, P. Y.; He, D. S.; Chen, Y. J.; Wang, D. S.; Niu, Z. Q.; Wu, Y.; Li, Y. D. Kinetically controlling surface structure to construct defect-rich intermetallic nanocrystals: Effective and stable catalysts. *Adv. Mater.* **2016**, *28*, 2540–2546.
[103] Wu, H. H.; Li, H. B.; Zhao, X. F.; Liu, Q. F.; Wang, J.; Xiao, J. P.; Xie, S. H.; Si, R.; Yang, F.; Miao, S. et al. Highly doped and exposed Cu(I)–N active sites within graphene towards efficient oxygen reduction for zinc–air batteries. *Energy Environ. Sci.* **2016**, *9*, 3736–3745.
[104] Zhang, H. N.; Li, J.; Xi, S. B.; Du, Y. H.; Hai, X.; Wang, J. Y.; Xu, H. M.; Wu, G.; Zhang, J.; Lu, J. et al. A graphene-supported single-atom FeN_5 catalytic site for efficient electrochemical CO_2 reduction. *Angew. Chem., Int. Ed.* **2019**, *58*, 14871–14876.
[105] Wang, X. Q.; Chen, Z.; Zhao, X. Y.; Yao, T.; Chen, W. X.; You, R.; Zhao, C. M.; Wu, G.; Wang, J.; Huang, W. X. et al. Regulation of coordination number over single Co sites: Triggering the efficient electroreduction of CO_2. *Angew. Chem., Int. Ed.* **2018**, *57*, 1944–1948.
[106] Pan, Y.; Chen, Y. J.; Wu, K. L.; Chen, Z.; Liu, S. J.; Cao, X.; Cheong, W. C.; Meng, T.; Luo, J.; Zheng, L. R. et al. Regulating the coordination structure of single-atom Fe-N_xC_y catalytic sites for benzene oxidation. *Nat. Commun.* **2019**, *10*, 4290.
[107] Qu, Y. T.; Li, Z. J.; Chen, W. X.; Lin, Y.; Yuan, T. W.; Yang, Z. K.; Zhao, C. M.; Wang, J.; Zhao, C.; Wang, X. et al. Direct transformation of bulk copper into copper single sites via emitting and trapping of atoms. *Nat. Catal.* **2018**, *1*, 781–786.
[108] Wei, S. J.; Li, A.; Liu, J. C.; Li, Z.; Chen, W. X.; Gong, Y.; Zhang, Q. H.; Cheong, W. C.; Wang, Y.; Zheng, L. R. et al. Direct observation of noble metal nanoparticles transforming to thermally stable single atoms. *Nat. Nanotechnol.* **2018**, *13*, 856–861.
[109] Ke, J.; Zhu, W.; Jiang, Y. Y.; Si, R.; Wang, Y. J.; Li, S. C.; Jin, C. H.; Liu, H. C.; Song, W. G.; Yan, C. H. et al. Strong local coordination structure effects on subnanometer PtO_x clusters over CeO_2 nanowires probed by low-temperature CO oxidation. *ACS Catal.* **2015**, *5*, 5164–5173.
[110] Nan, B.; Hu, X. C.; Wang, X.; Jia, C. J.; Ma, C.; Li, M. X.; Si, R. Effects of multiple platinum species on catalytic reactivity distinguished by electron microscopy and X-ray absorption spectroscopy techniques. *J. Phys. Chem. C* **2017**, *121*, 25805–25817.
[111] Ren, Y. J.; Tang, Y.; Zhang, L. L.; Liu, X. Y.; Li, L.; Miao, S.; Su, D. S.; Wang, A. Q.; Li, J.; Zhang, T. Unraveling the coordination structure-performance relationship in Pt_1/Fe_2O_3 single-atom catalyst. *Nat. Commun.* **2019**, *10*, 4500.
[112] Ye, T. N.; Xiao, Z. W.; Li, J.; Gong, Y. T.; Abe, H.; Niwa, Y.; Sasase, M.; Kitano, M.; Hosono, H. Stable single platinum atoms trapped in sub-nanometer cavities in $12CaO{\cdot}7Al_2O_3$ for chemoselective hydrogenation of nitroarenes. *Nat. Commun.* **2020**, *11*, 1020.
[113] Shen, G. Q.; Zhang, R. R.; Pan, L.; Hou, F.; Zhao, Y. J.; Shen, Z. Y.; Mi, W. B.; Shi, C. X.; Wang, Q. F.; Zhang, X. W. et al. Regulating the spin state of Fe^{III} by atomically anchoring on ultrathin titanium dioxide for efficient oxygen evolution electrocatalysis. *Angew. Chem., Int. Ed.* **2020**, *59*, 2313–2317.
[114] Zhao, G. F.; Yang, F.; Chen, Z. J.; Liu, Q. F.; Ji, Y. J.; Zhang, Y.; Niu, Z. Q.; Mao, J. J.; Bao, X. H.; Hu, P. J. et al. Metal/oxide interfacial effects on the selective oxidation of primary alcohols. *Nat. Commun.* **2017**, *8*, 14039.
[115] Lei, Y.; Liu, B.; Lu, J. L.; Libera, J. A.; Greeley, J. P.; Elam, J. W. Effects of chlorine in titanium oxide on palladium atomic layer deposition. *J. Phys. Chem. C* **2014**, *118*, 22611–22619.

[116] Yin, X.; Utetiwabo, W.; Sun, S. H.; Lian, Y. M.; Chen, R. J.; Yang, W. Incorporation of CeF_3 on single-atom dispersed Fe/N/C with oxophilic interface as highly durable electrocatalyst for proton exchange membrane fuel cell. *J. Catal.* **2019**, *374*, 43–50.

[117] Wang, J.; Huang, Z. Q.; Liu, W.; Chang, C. R.; Tang, H. L.; Li, Z. J.; Chen, W. X.; Jia, C. J.; Yao, T.; Wei, S. Q. et al. Design of N-coordinated dual-metal sites: A stable and active Pt-free catalyst for acidic oxygen reduction reaction. *J. Am. Chem. Soc.* **2017**, *139*, 17281−17284.

[118] Lu, Z. Y.; Wang, B.; Hu, Y. F.; Liu, W.; Zhao, Y. F.; Yang, R. O.; Li, Z. P.; Luo, J.; Chi, B.; Jiang, Z. et al. An isolated zinc–cobalt atomic pair for highly active and durable oxygen reduction. *Angew. Chem., Int. Ed.* **2019**, *58*, 2622–2626.

[119] Zhang, L.; Si, R. T.; Liu, H. S.; Chen, N.; Wang, Q.; Adair, K.; Wang, Z. Q.; Chen, J. T.; Song, Z. X.; Li, J. J. et al. Atomic layer deposited Pt-Ru dual-metal dimers and identifying their active sites for hydrogen evolution reaction. *Nat. Commun.* **2019**, *10*, 4936.

[120] Bai, L. C.; Hsu, C. S.; Alexander, D. T. L.; Chen, H. M.; Hu, X. L. A cobalt–iron double-atom catalyst for the oxygen evolution reaction. *J. Am. Chem. Soc.* **2019**, *141*, 14190–14199.

[121] Nguyen, L.; Zhang, S. R.; Tan, L.; Tang, Y.; Liu, J. Y.; Tao, F. F. Ir_1Zn_n bimetallic site for efficient production of hydrogen from methanol. *ACS Sustainable Chem. Eng.* **2019**, *7*, 18793−18800.

[122] Han, X. P.; Ling, X. F.; Yu, D. S.; Xie, D. Y.; Li, L. L.; Peng, S. J.; Zhong, C.; Zhao, N. Q.; Deng, Y. D.; Hu, W. B. Atomically dispersed binary Co-Ni sites in nitrogen-doped hollow carbon nanocubes for reversible oxygen reduction and evolution. *Adv. Mater.* **2019**, *31*, 1905622.

[123] Wu, K. L.; Chen, X.; Liu, S. J.; Pan, Y.; Cheong, W. C.; Zhu, W.; Cao, X.; Shen, R. G.; Chen, W. X.; Luo, J. et al. Porphyrin-like Fe-N_4 sites with sulfur adjustment on hierarchical porous carbon for different rate-determining steps in oxygen reduction reaction. *Nano Res.* **2018**, *11*, 6260–6269.

[124] Mun, Y.; Lee, S.; Kim, K.; Kim, S.; Lee, S.; Han, J. W.; Lee, J. Versatile strategy for tuning ORR activity of a single Fe-N_4 site by controlling electron-withdrawing/donating properties of a carbon plane. *J. Am. Chem. Soc.* **2019**, *141*, 6254–6262.

[125] Chen, Y. J.; Ji, S. F.; Zhao, S.; Chen, W. X.; Dong, J. C.; Cheong, W. C.; Shen, R. A.; Wen, X. D.; Zheng, L. R.; Rykov, A. I. et al. Enhanced oxygen reduction with single-atomic-site iron catalysts for a zinc-air battery and hydrogen-air fuel cell. *Nat. Commun.* **2018**, *9*, 5422.